Real-Time Hologram Rendering from Optically-Acquired Interferograms webinar

Exploring cell structure and dynamics with non-invasive quantitative phase-digital holographic microscopy

Pierre Marquet, PhD, MD

CERVO Brain Research Centre

Centre for optics, photonics and laser

Université Laval, Québec

collaboration with

Centre de Neurosciences Psychiatriques
University of Lausanne

Biomolecular Screening Facility
École Polytechnique Fédérale de Lausanne

Laboratoire de Neuroénergétique et de Dynamique Cellulaire
Brain and Mind Institute, EPFL

Webinar, OSA September 8 2017

ÉCOLE POLYTECHNIQUE FÉDÉRALE DE LAUSANNE

CHUV

UNIL | Université de Lausanne
Faculté de biologie et de médecine

CENTRE DE RECHERCHE CERVO BRAIN RESEARCH CENTRE QUÉBEC

Canada Excellence Research Chairs
Chaires d'excellence en recherche du Canada

UNIVERSITÉ LAVAL

Motivations

- Recovery of the full complex scattered wavefront i.e. the amplitude and the phase of the wave field which has interacted with a specimen

  - Material sciences
    - Surface topography and finish , defect inspection, MEMS analysis
    - Micro optical components , microfluidic devices
    - Defects or particles inside transparent samples
    - Characterization of micro optics (shape, refractive index, etc.).

  - Life sciences
    - visualization of transparent specimen including living cells
    - Non-invasive exploration of cell structure and dynamics

Bright field-phase contrast

$$\boldsymbol{O}(\boldsymbol{r}) = \boldsymbol{U}_{\text{inc}}(\boldsymbol{r}) \cdot T(\boldsymbol{r}) =$$
$$U_0 \exp\{i\varphi(\boldsymbol{r})\} \exp\{i\phi(\boldsymbol{r})\}$$

$$\left|\boldsymbol{O}(\boldsymbol{r})\right|^2 = \left|\boldsymbol{U}_{inc}(\boldsymbol{r}) \cdot T(\boldsymbol{r})\right|^2 = U_0^2$$

Phase-contrast & Bright-field microscopy

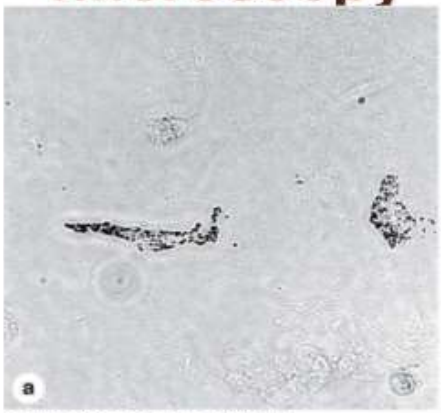

Bright-field microscopy: without fixation and staining, only the two pigment cells can be seen.

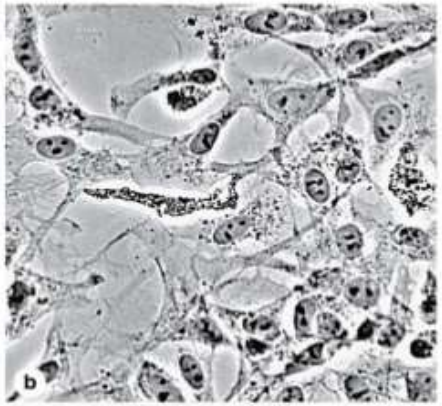

Phase-contrast microscopy: cell boundaries, nuclei, and cytoplasmic structures with different refractive indices affect in-phase light differently and produce an image of these features in all the cells.

Frits Zernike (1942). "Phase contrast, a new method for the microscopic observation of transparent objects part I". *Physica*. **9** (7): 686–698

Phase contrast microscope

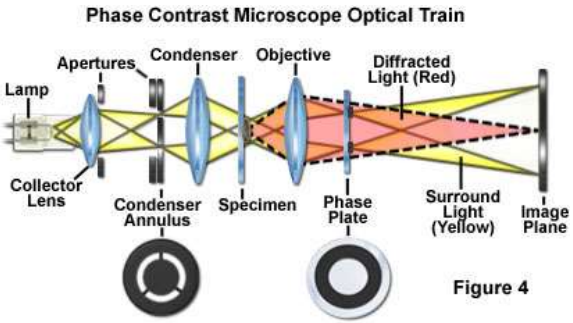

Phase artefacts, image distortion

- Halo
- shade off

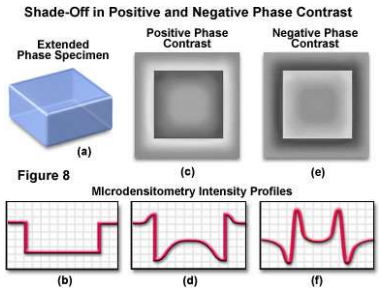

Leitz Mach-Zehnder, interference microscope

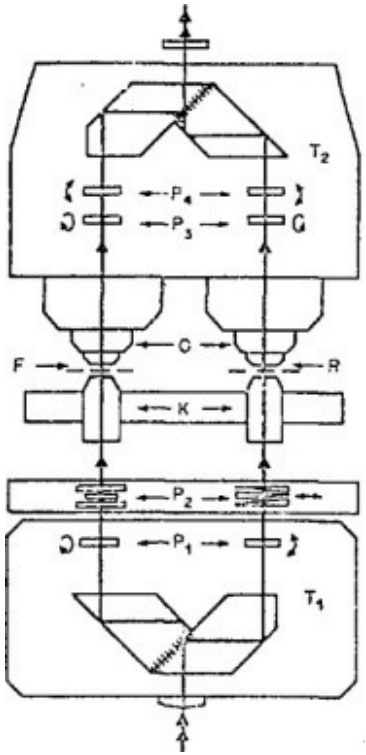

Barer, Nature, 1952

holography principle

enabling the full-field recovery represents a conductive approach for the development of quantitative phase imaging

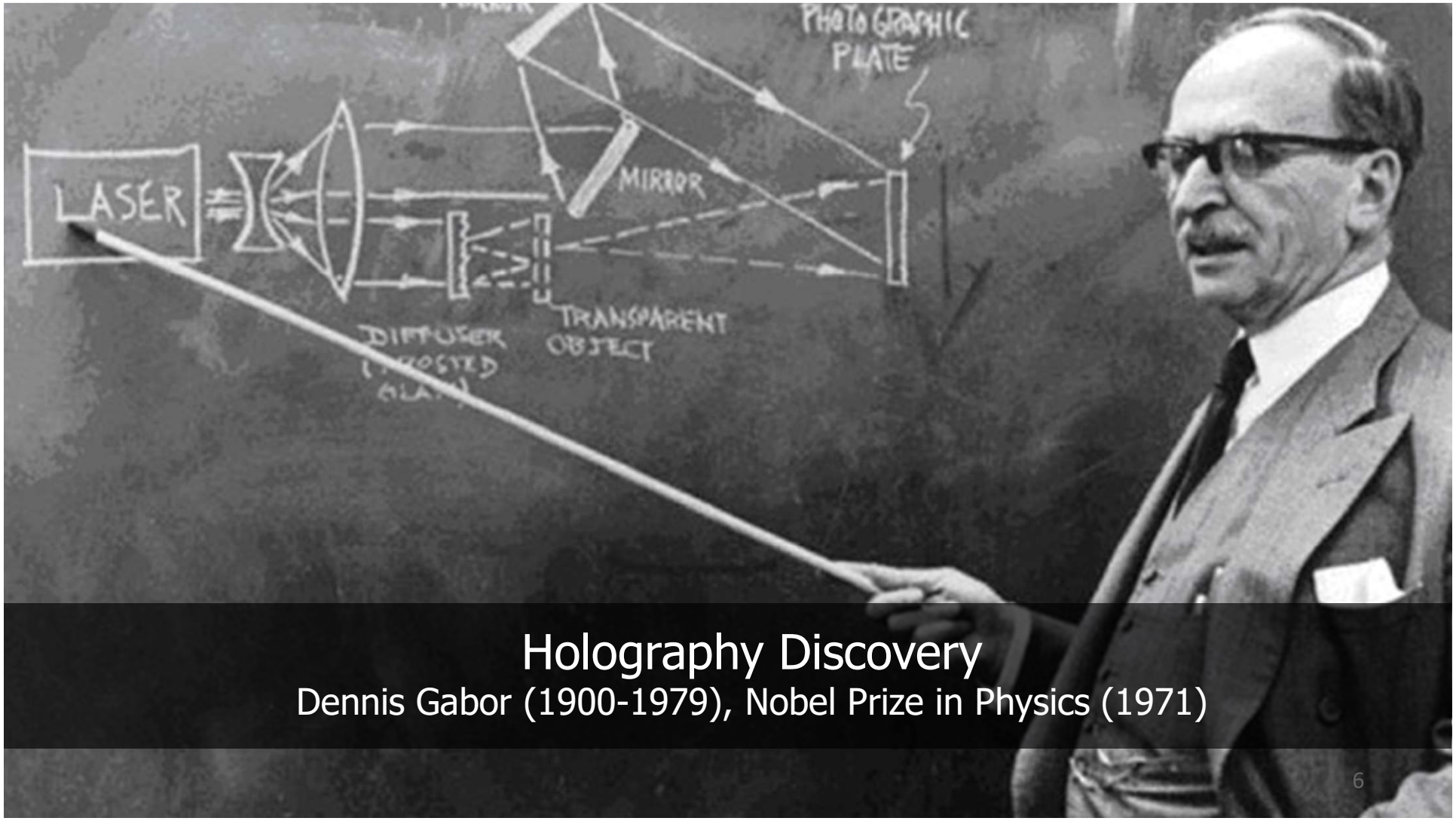

Holography Discovery

Dennis Gabor (1900-1979), Nobel Prize in Physics (1971)

Principle of classical holography

Recording the hologram

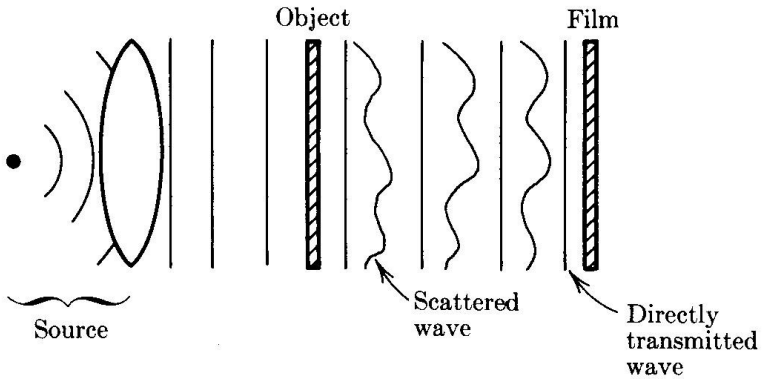

Reconstruction of the wavefront of the original object

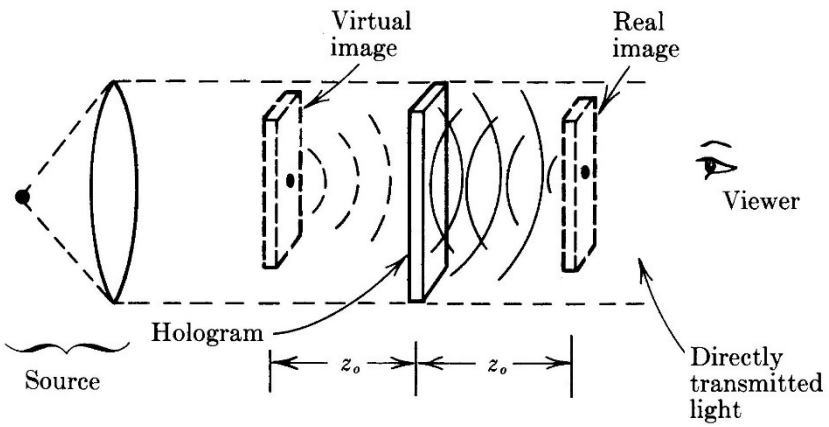

Adapted from J.W. Goodman, Introduction to Fourier optics

Holography gained new life with the advent of the laser

Leith and Upatnieks (1962) applied laser light to holography and fixed the twin image issue

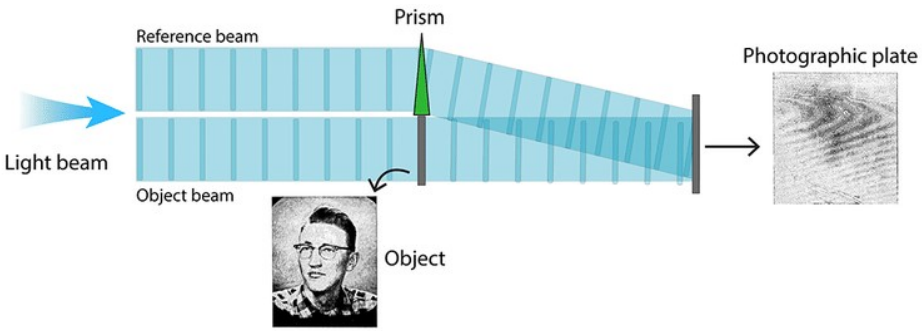

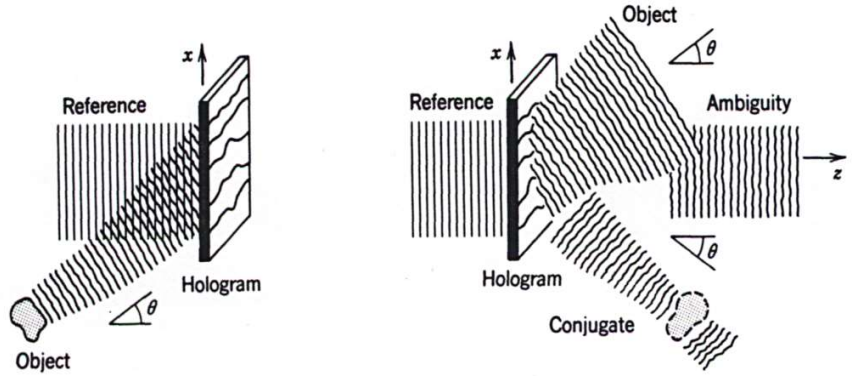

$$I_H(x,y) = |\boldsymbol{R}+\boldsymbol{O}|^2 = |R|^2 + |O|^2 + \boldsymbol{R}^*\boldsymbol{O} + \boldsymbol{R}\boldsymbol{O}^*$$

$$= \underbrace{|R|^2 + |O|^2}_{\text{Zero-order}} + \underbrace{\boldsymbol{R}^*\boldsymbol{O}}_{\text{1-order}} + \underbrace{\boldsymbol{R}\boldsymbol{O}^*}_{\text{-1-order}}$$

$$\boldsymbol{O}(x,t) = O_0 \exp\{i\varphi(x,t)\}$$

From optical holography to digital holography

Technological advances both in CCD camera resolution and computer speed have recently enabled digital holography

- J.W. Goodman and R. W. Laurence proposed for the first time in 1967 the idea to reconstruct a hologram with a computer (.W. Goodman and R. D. Lawrence, ’ Appl. Phys. Lett. **11**, 77-79)
- The use of numerical technique for the creation of so-called computer generated holograms was demonstrated by B.R. Brown and A. W. Lohman in 1966
- M. A. Kronrod, N. S. Merzlyakov, and L. P. Yaroslavskii…

From optical holography to digital holography

- In 1994 U. Schnars and W. Jüptner have reported the numerical reconstruction of a Fresnel off-axis hologram using a CCD camera Appl. Opt. **33**, 179-181 (1994).

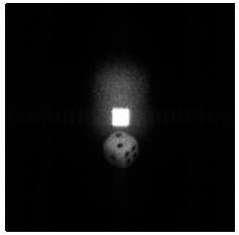

Figure 8. Numerical intensity reconstruction.

Application to quantitative phase microscopy:

- **Time domain:** phase shifting holography: needs the acquisition of four holograms : Y. Yamaguchi 1997+2001 , F. Dubois 2001
- **Space domain:** off-axis reference wave : needs the acquisition of a single hologram : E. Cuche, P. Marquet, C. Depeursinge, 1999
- **Spatio-temporal domain** proposed by G. Indebetouw 2001, operating in incoherent and coherent modes
- **In line digital holography** proposed by H. J. Kreuzer , 2001
- …

digital holographic/interferometric configurations

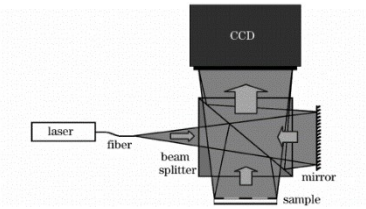

V. R. Singh et al. Opt. Letters 2009

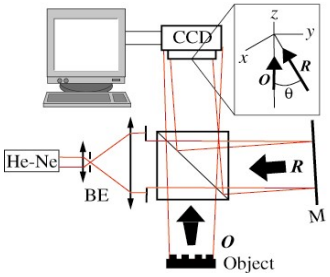

Cuche et al. appl. Opt.1999

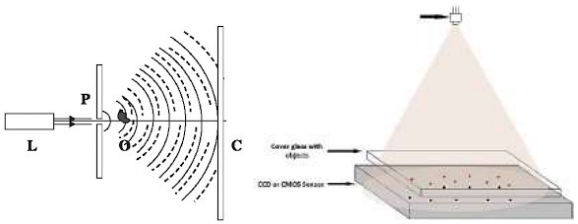

W. Xu et al. PNAS, 2001

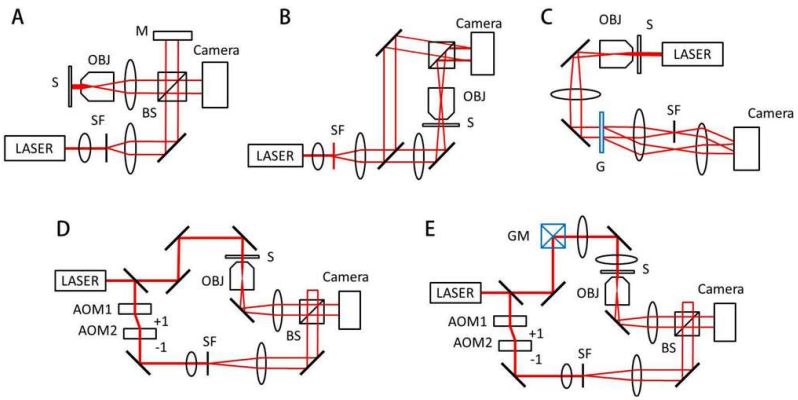

K. Lee, Sensors, 2013

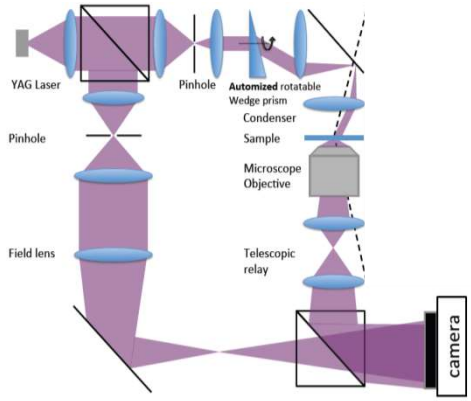

Cotte et al. Nature photonics (2013)

Digital holographic and interferometric approaches to develop quantitative phase imaging

D. Psaltis
Y. Park
O. Matoba
R. Chmelik
J. Garcia
P. Ferraro
F. Dubois
C. Yang
P. T. C. So
S. Thibaut
C. Sheppard
G. Barbastathis
C. Depeursinge
A. P. Wax
M. Gross
N. T. Shaked
C. Boccara
G. Von Bally
G. Popescu
Z. Zalevsky
V. Mico
C. Fournier
B. Kemper
G. Pedrini
P. Marquet
M.S. Feld
M. K. Kim
B. Javidi
P. Picart
I. Moon
L. Waller
M. Atlan
O. Haeberlé
H. Tiziani
P. Bon
M. Brunel
A. Ozcan
N. Pavillon
A. Sentenac

And many others…

Off-axis digital holographic microscopy to develop quantitative phase imaging

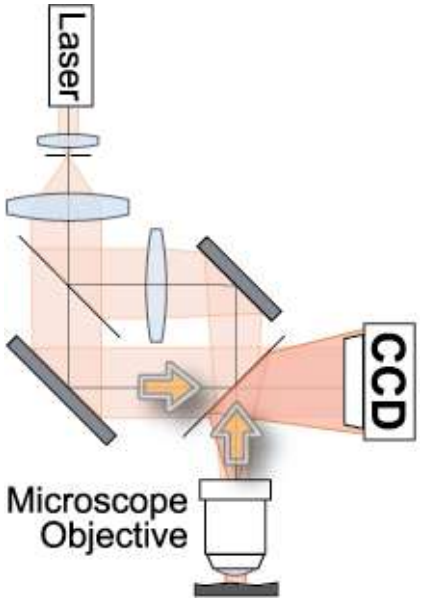

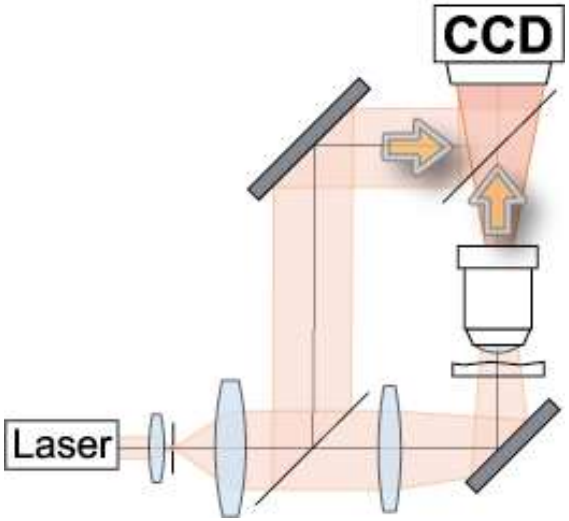

The problem of hologram sampling

Digital camera: pixel density
Pixel size: 3.x3. To 7.x 7. Microns

Approximately 10-50 x less dense than photographic film!

Hologram
(512×512 pixels)

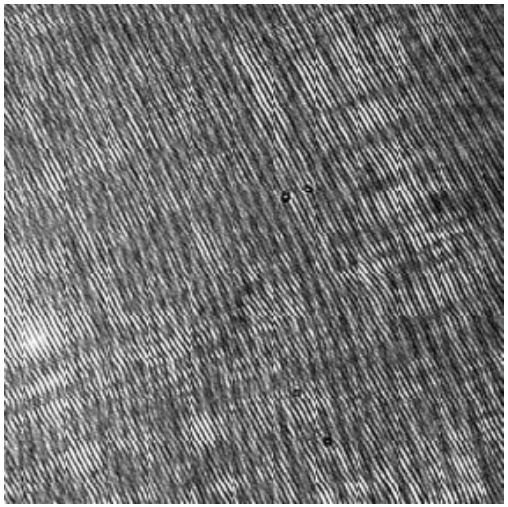

$$I_H(x,y) = |\boldsymbol{R}+\boldsymbol{O}|^2 = |R|^2 + |O|^2 + \boldsymbol{R}^*\boldsymbol{O} + \boldsymbol{R}\boldsymbol{O}^*$$

$$= \underbrace{|R|^2 + |O|^2}_{\text{Zero-order}} + \underbrace{\boldsymbol{R}^*\boldsymbol{O}}_{\text{1-order}} + \underbrace{\boldsymbol{R}\boldsymbol{O}^*}_{\text{-1-order}}$$

and consequences on image resolution

Lensless off-axis holography

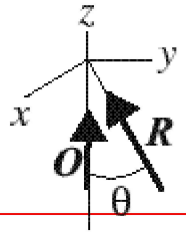

- *Off-axis reference:* $\boldsymbol{R}(x,y) = \sqrt{I_r}\,\exp\{ik\sin\theta x\}$

$$\Psi(x,y) = R_D \cdot I_H = R_D \cdot \Big[\underbrace{I_R + I_O}_{\text{Zero order}} + \underbrace{\sqrt{I_R}\exp(-ik\sin\theta x)\,O}_{\text{Virtual image}} + \underbrace{\sqrt{I_R}\exp(ik\sin\theta x)\,O^*}_{\text{Real image}} \Big]$$

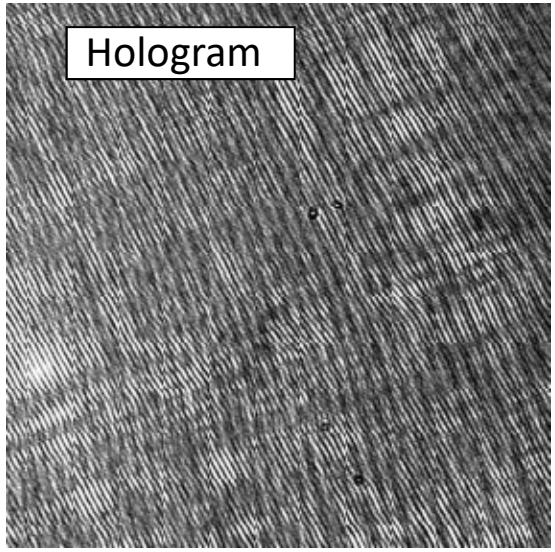

FFT

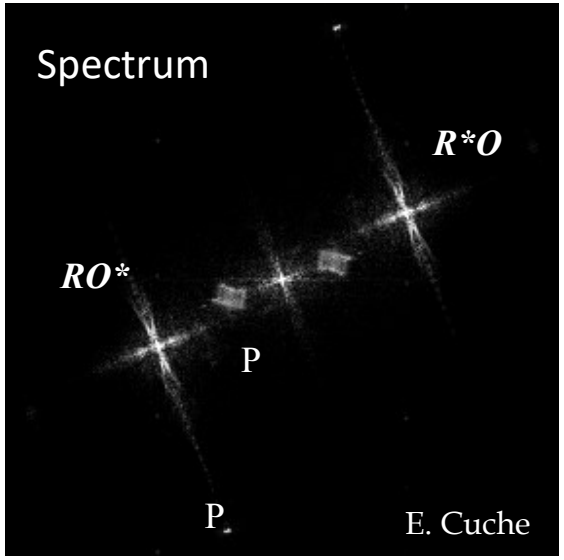

et

Numerical Reconstruction
Principle and Geometry

Hologram intensity
$I_H(x,y)$

Numerical calculation
of scalar diffraction

Reconstructed wave front
$\Psi(\xi,\eta)$

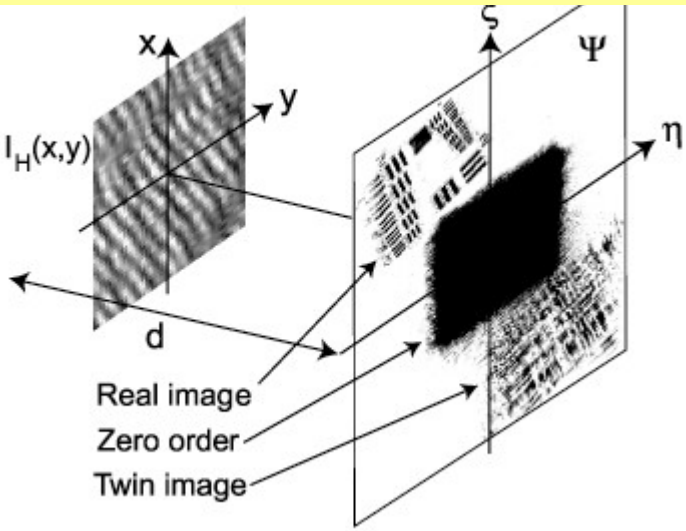

- d Reconstruction distance

Propagation of the wavefront from the hologram plane to the reconstruction plane

$$\Psi_d(\xi,\eta) = \frac{e^{i2\pi d/\lambda}}{i\lambda d} \cdot e^{\frac{i\pi}{\lambda d}(\xi^2+\eta^2)} \iint \boldsymbol{R}(x,y) I_H(x,y)\, e^{\frac{i\pi}{\lambda d}(x^2+y^2)}\, e^{\frac{i\pi}{\lambda d}(x\xi+y\eta)}\, dxdy$$

Fourier transform $\boldsymbol{R}(x,y) I_H(x,y) \exp\left\{\frac{i\pi}{\lambda d}(x^2+y^2)\right\}$ spatial frequencies $\frac{\xi}{\lambda d}$ $\frac{\eta}{\lambda d}$

Fresnel approximation

Example

Reconstructed image

Hologram (512×512 pixels)

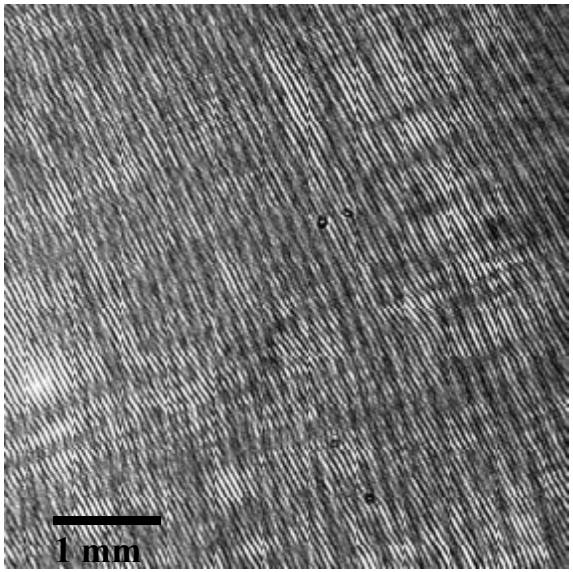

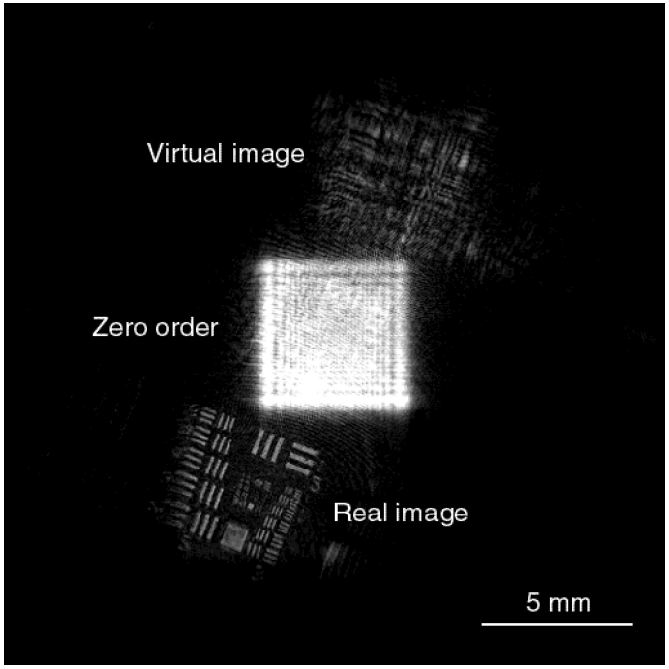

Spatial filtering

recorded hologram

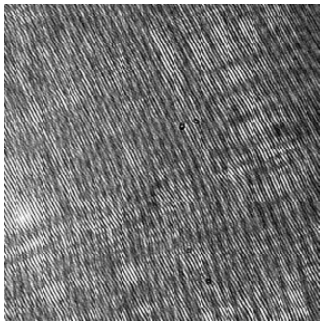

FFT

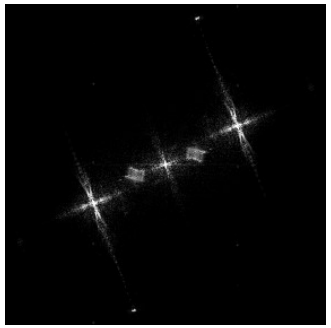

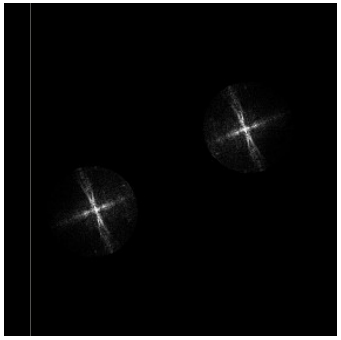

FFT^{-1}

Filtered hologram

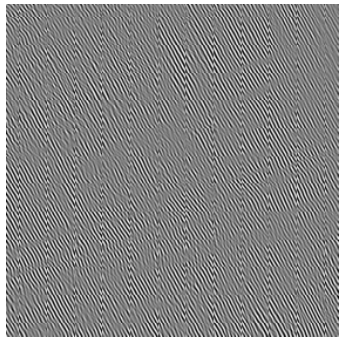

Numerically reconstructed images

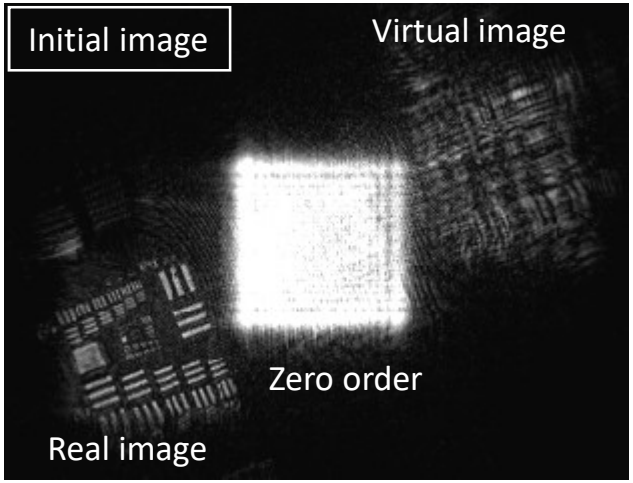

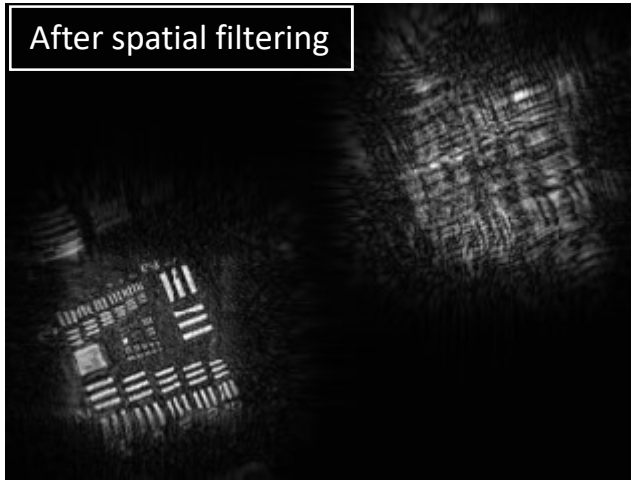

- Zero order elimination ➲ Enhanced signal/background ratio.
- Parasitic reflection elimination ➲ Noise reduction.

Twin image elimination

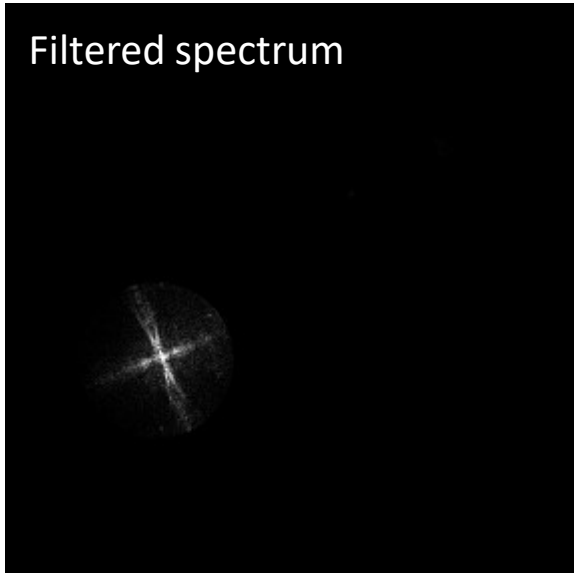

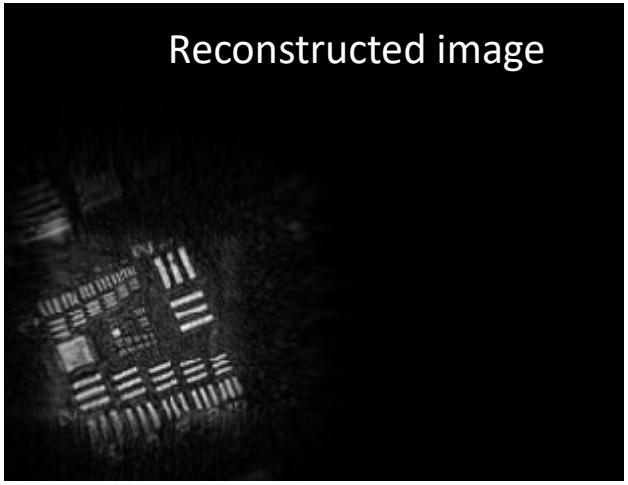

!! Symmetry of the spectrum is lost

Criteria for spatial filtering

Off-axis hologram

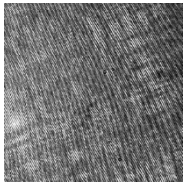

$$\psi_1(x,y,z=0) = tI_r\boldsymbol{A}$$

$$\psi_2(x,y,z=0) = t\left|O(x,y)\right|^2\boldsymbol{A}$$

$$\psi_3(x,y,z=0) = tR_0\boldsymbol{O}(x,y)\exp(-ik\sin\theta x)\boldsymbol{A}$$

$$\psi_4(x,y,z=0) = tR_0\boldsymbol{O}^*(x,y)\exp(ik\sin\theta x)\boldsymbol{A}$$

$$\boldsymbol{A}(z) = A_0\exp(ikz)$$

$$\boldsymbol{R}(x,z) = R_0\exp(i(k\sin\theta x + k\cos\theta z)$$

$$\boldsymbol{G}(k_x,k_y) = \Im\{\mathrm{I_H}(x,y)\} = \int_{-\infty}^{\infty}dx\int_{-\infty}^{\infty}dy\ \mathrm{I_H}(x,y)\exp(-i(k_x x + k_y y))$$

$$\boldsymbol{G_o}(k_x,k_y) = \Im\{\boldsymbol{O}(x,y,z=0)\}$$

B =spatial bandwidth of O(x,y)

* = autocorrelation product

Hologram spectrum

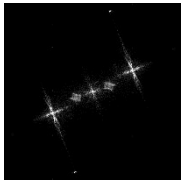

$$G_1(k_x,k_y) = I_r\delta(k_x)\delta(k_y)$$

$$\boldsymbol{G_2}(k_x,k_y) = \boldsymbol{G_o}(k_x,k_y) * \boldsymbol{G_o}(k_x,k_y)$$

$$\boldsymbol{G_3}(k_x,k_y) = R_0\boldsymbol{G_o}(k_x + k\sin\theta, k_y)$$

$$\boldsymbol{G_4}(k_x,k_y) = R_0\boldsymbol{G_o^*}(-k_x - k\sin\theta, -k_y)$$

,

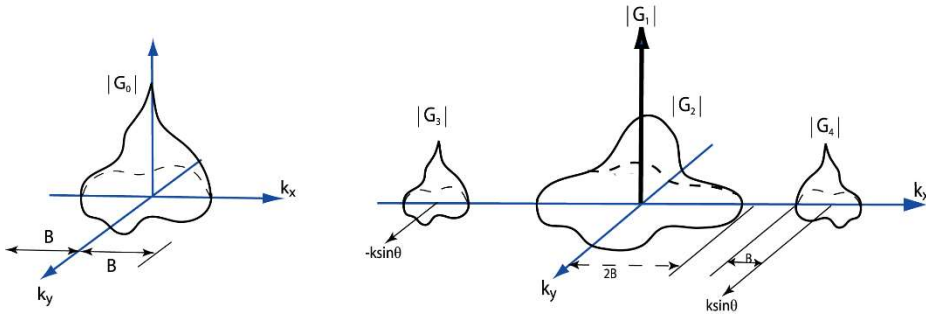

Adapted from J.W. Goodman, Introduction to Fourier optics

a b

$$k\sin\theta \geq 3B \rightarrow \sin\theta \geq 3B\frac{\lambda}{2\pi}$$

$$B_H = 4B$$

Wave front reconstruction: need for adjustment

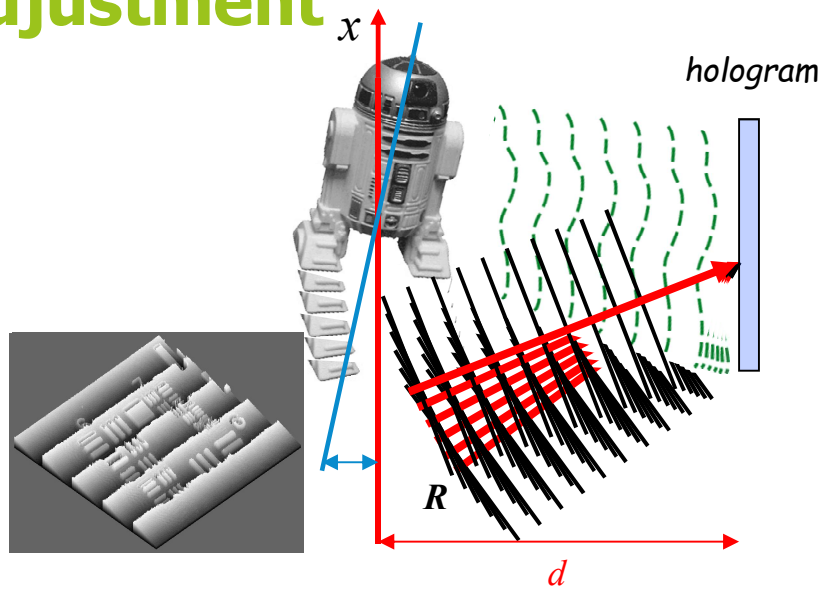

First Ajustement 1

Tilt angle for the image positioning

$$\text{tilt} = \sin\theta x + \cos\theta z$$

Propagation of the wavefront from the hologram plane to the reconstruction plane

$$\Psi_d(\xi,\eta) = \frac{e^{i2\pi d/\lambda}}{i\lambda d} \cdot e^{\frac{i\pi}{\lambda d}\left(\xi^2+\eta^2\right)} \iint \boldsymbol{R}(x,y) I_H(x,y)\, e^{\frac{i\pi}{\lambda d}\left(x^2+y^2\right)}\, e^{\frac{i\pi}{\lambda d}(x\xi+y\eta)}\, dxdy$$

$$\boldsymbol{R}(x,z) = R_0 \exp(i(k\sin\theta x + k\cos\theta z)$$

Holographic microscopy configuration

$$U_i(x_i, y_i) = \int_{-\infty}^{\infty}\int h(x_i, y_i; x_0, y_0) U_0(x_0, y_0) dx_0 dy_0$$

Fresnel diffraction to account propagation

$$h(x_i, y_i; x_0, y_0) =$$

$$K(x_i, y_i) \int_{-\infty}^{+\infty}\int P(x, y) \exp\left\{-i \frac{2\pi}{\lambda(d_i - f)}\left[(x_i - Mx_0)x + (y_i - My_0)y\right]\right\} dxdy$$

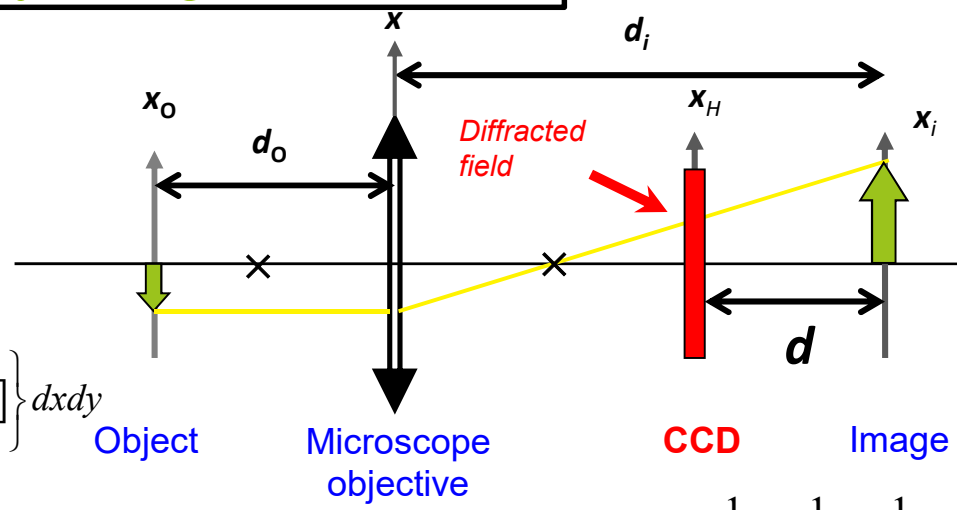

$$\frac{1}{f} = \frac{1}{d_o} + \frac{1}{d_i}$$

(x, y) Coordinates in the lens pupil plan

$h(x_i, y_i; x_0, y_0)$ Impulse response of the system

$P(x, y)$ Lens pupil

$K(x_i, y_i)$ Complex function depending of the MO characteristics and corresponding to a wavefront curvature given by

$$\exp\left\{i \frac{k}{2(d_i - f)}(x_i^2 + y_i^2)\right\}$$

Digital correction of phase aberration

Wave front deformation:

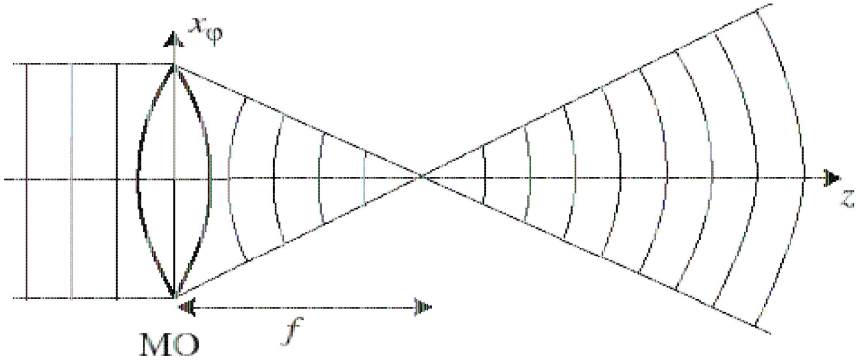

(spherical lens, Fresnel approximation)

$$\psi_{corr}(\xi,\eta) = \exp\left\{\frac{i\pi}{\lambda D}(\xi^2+\eta^2)\right\}\psi(\xi,\eta)$$

D= (f, object-objective distance)

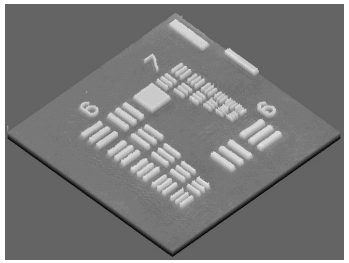

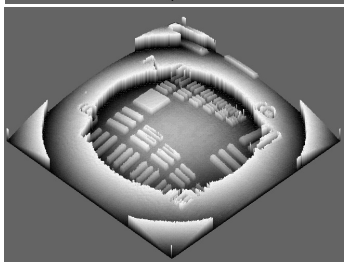

Introduction of phase aberrations

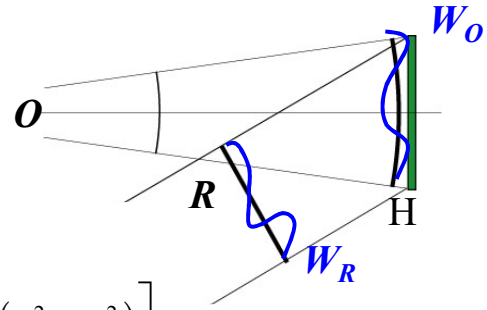

- Hologram plane:

Reference wave $\boldsymbol{R}(x,y) = |\boldsymbol{R}| \exp\left[i \frac{2\pi}{\lambda} \left(k_x \cdot x + k_y \cdot y \right) \right]$

Object wave $\boldsymbol{O}(x,y) = |\boldsymbol{O}(x,y)| \exp[i\varphi(x,y)] \exp\left[\frac{i\pi}{\lambda D} \left(x^2 + y^2 \right) \right]$

Filtered hologram (keeping only the virtual term)

$$I_H^F = \boldsymbol{R} * \boldsymbol{O} = |\boldsymbol{R}| |\boldsymbol{O}| \exp[i\varphi(x,y)] \exp\left[-i \frac{2\pi}{\lambda} \left(k_x \cdot x + k_y \cdot y \right) \right] \exp\left[\frac{i\pi}{\lambda D} \left(x^2 + y^2 \right) \right] \exp\left[i \left(W_O - W_R \right) \right]$$

- *Propagation in Image plane :* *playing a role:*
  - *Phase delay*
  - *Tilt due to the reference wave propagation direction*
  - *Curvature induced by the MO*
  - *Aberrations terms*

T. Colomb et al. , “Numerical parametric lens for shifting, magnification, and complete aberration compensation in digital holographic microscopy”, JOSA, 2006
F. Monfort, et al., “Purely numerical compensation for microscope objective phase curvature in digital holographic microscopy: influence of digital phase mask position”, JOSA, 2006
T. Colomb, Total aberration compensation in digital holographic microscopy with a reference conjugated hologram, Opt. Express, 2006

Digital holographic microscopy with a ball lens

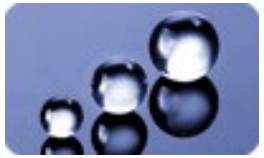

Without correction

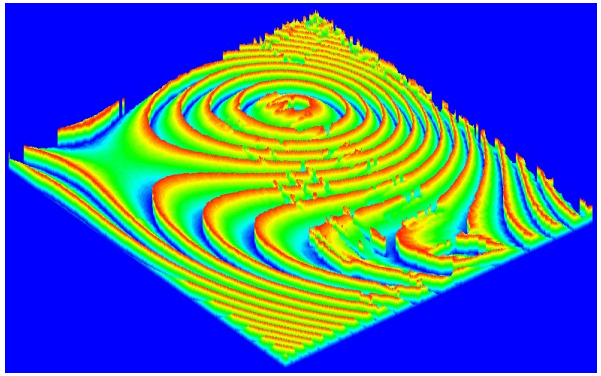

Aberration corrected

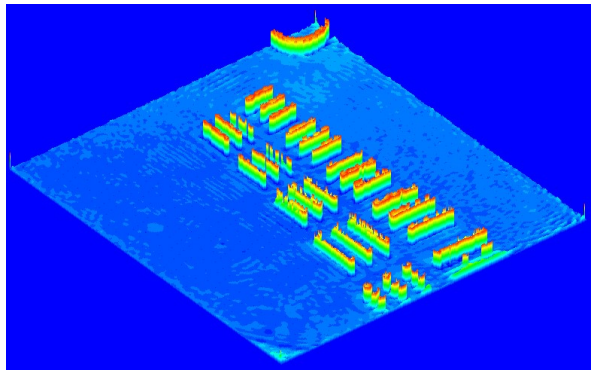

Classical microscopy

As « perfect » as possible

« stigmatic systems »

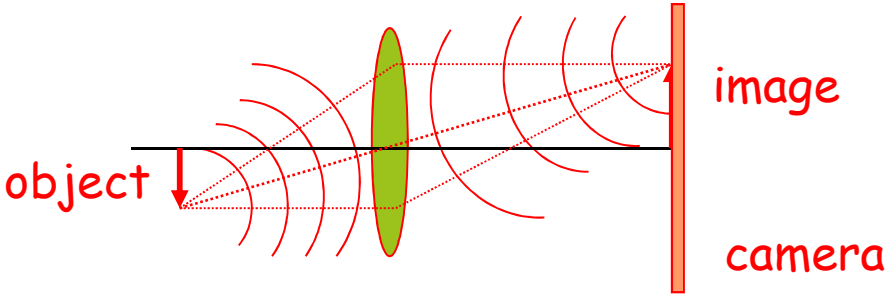

Digital Holographic Microscopy

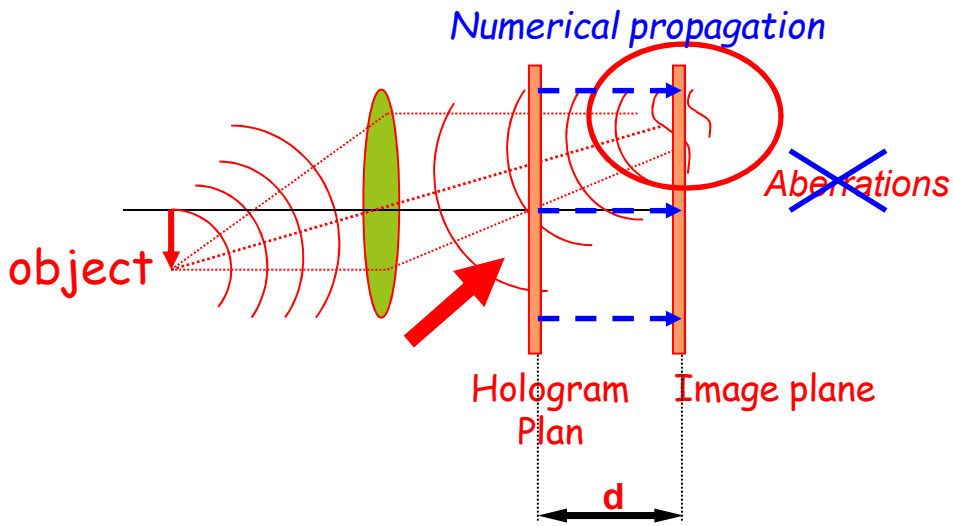

Colomb et al. *Opt. Exp.* 2006

A new generation of imaging techniques
can make use of « non-stigmatic systems »

- Numerical correction of aberration
- Extended depth of focus

d= numerical reconstruction distance

DHM unique property: Electronic Focusing

- Extended depth of field

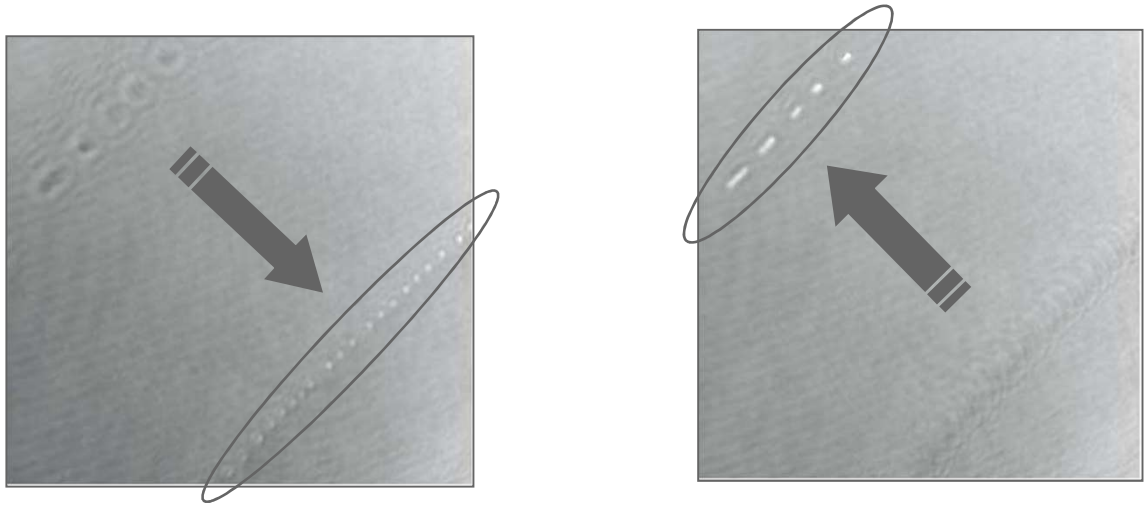

A single hologram taken in a few micro-seconds yields all the details by focusing digitally at various depths of field

Immunity to vibrations and motion blur !

Use a microscope objective !

Need for high N.A.!

Our choice: An approach with a microscope objective
To adapt the space -bandwidth product to the sampling capabilities of the electronic camera

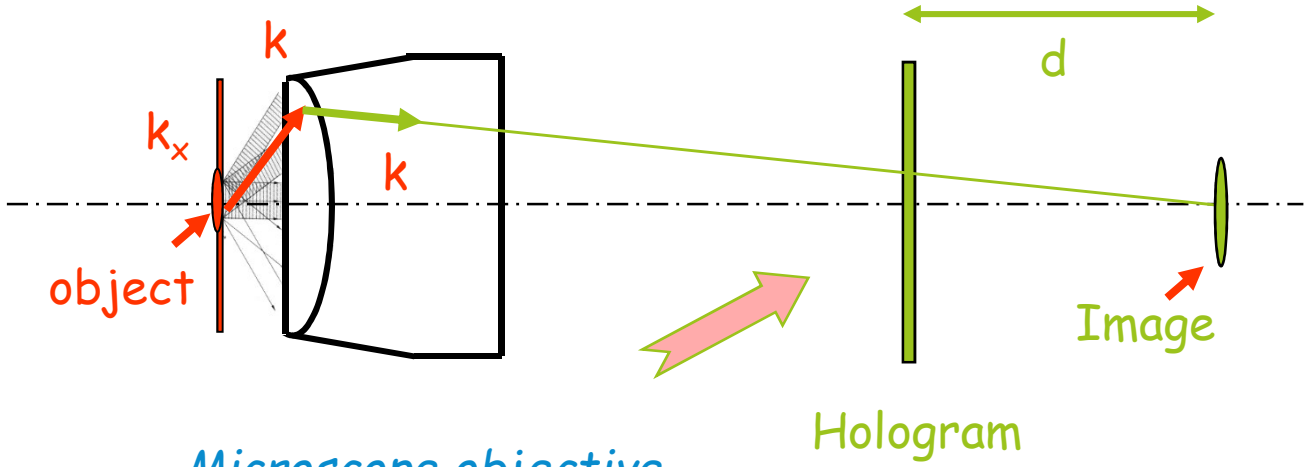

Propagating the wavefield from the hologram plane to the image plane will restore the image

Digital holography Microcopy

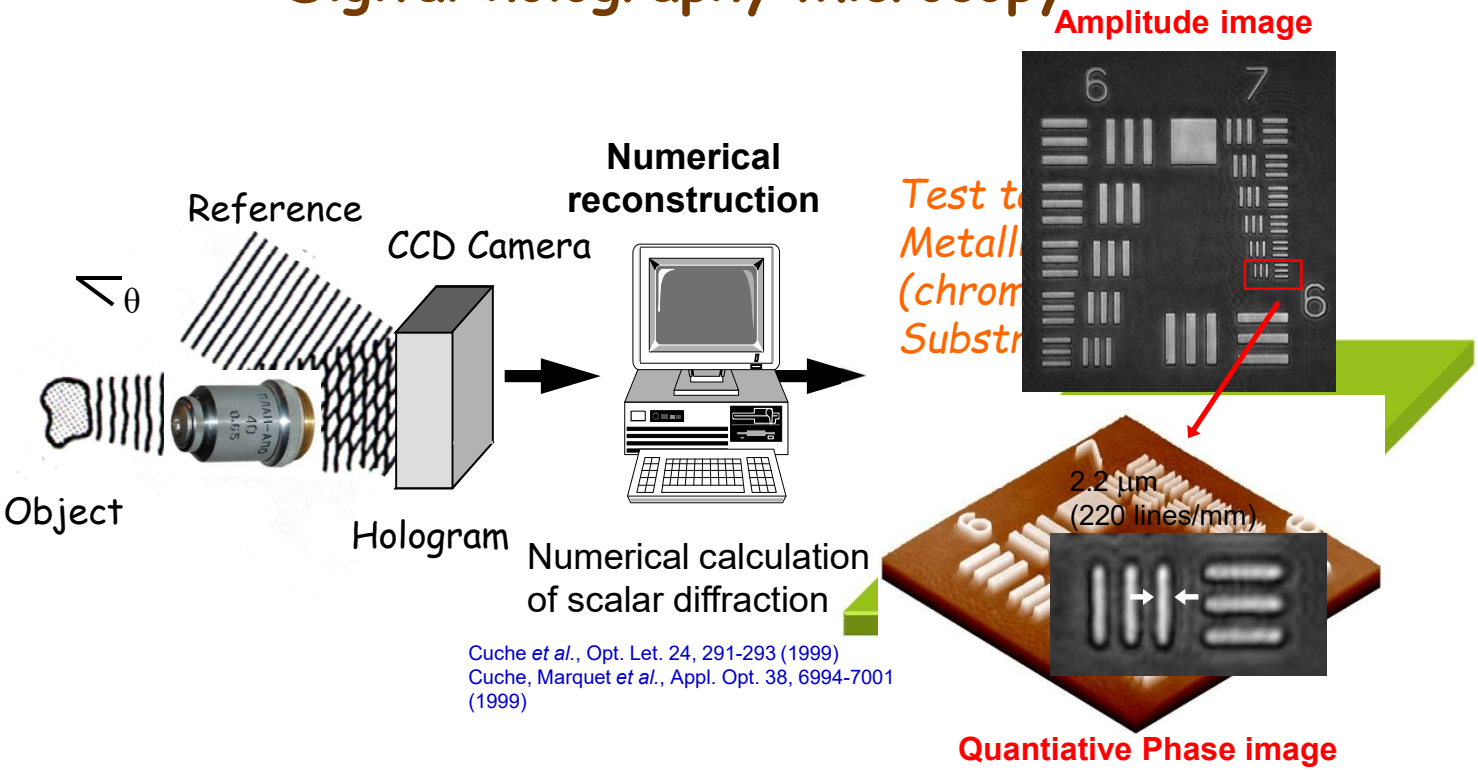

Cuche *et al.*, Opt. Let. 24, 291-293 (1999)
Cuche, Marquet *et al.*, Appl. Opt. 38, 6994-7001 (1999)

Advantages: High acquisition rate (camera-limited).
High reconstruction rate (25 images/sec)
Choice of the focalization plane
Numerical correction of phase aberration
Nanometric axial sensitivity

Sub-nanometer accuracy and sensitivity are achievable

Courtesy of Lyncée Tec

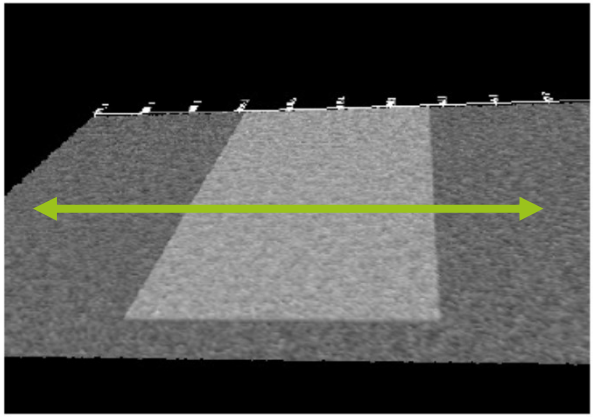

3D Image of a calibrated 8nm height metallic strip

Noise can be scaled down to the picometer range by averaging !

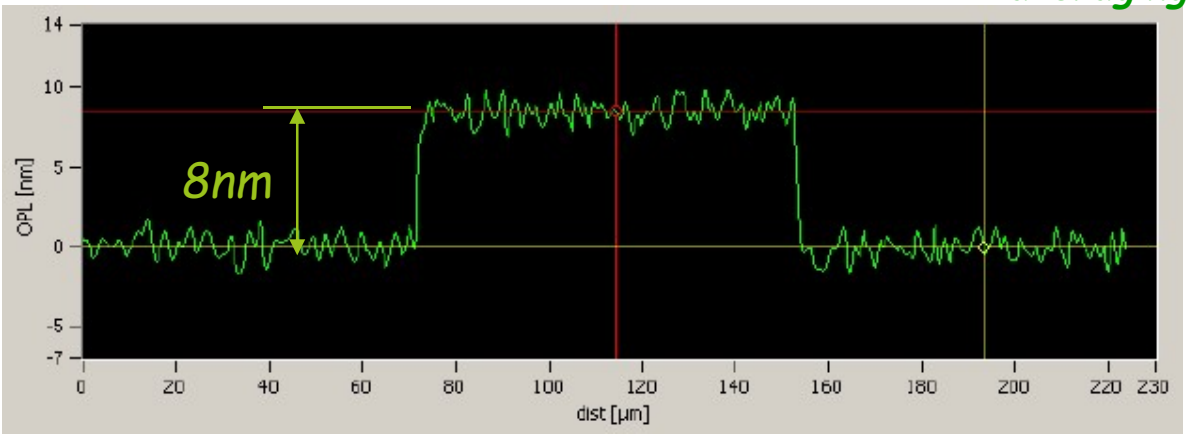

J. Kühn, et al., *Optics Express* 15, (2008)

Material Science Applications

DHM microscopes

DHM R1000

DHM T1000

https://www.lynceetec.com/

MOEMS: laser cavity

- Interference length = 0.35 micrometers
- Grey levels ⇒ nanometer resolution
- References to calculate the displacement

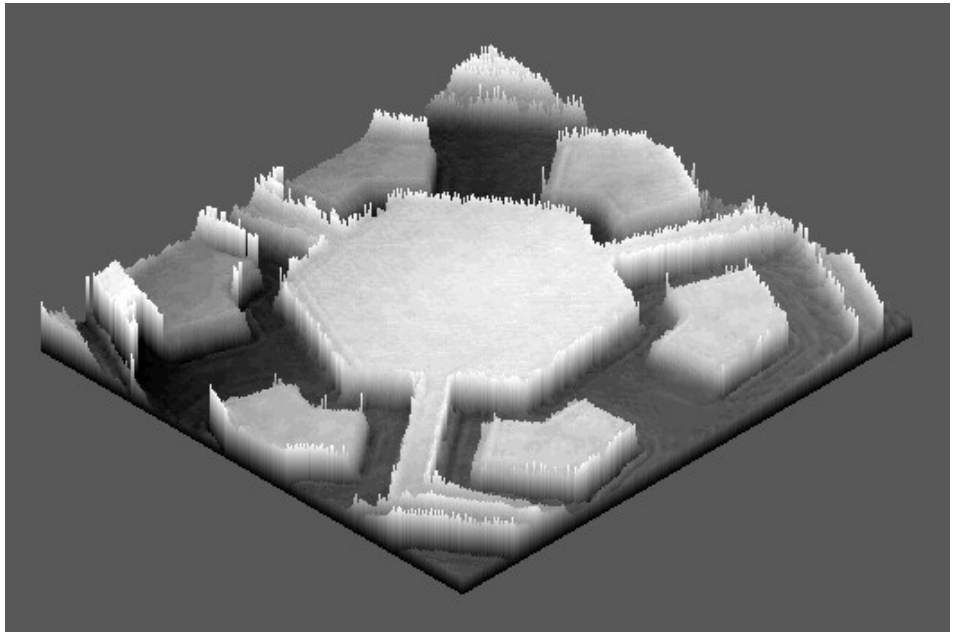

- Imaging time : 1/10 s

Membrane hysteresis

Goals of the measurement

- Measurements of hysteresis induced by the dipole alignment as a function of the applied voltage for increasing voltage amplitude
- Determination of breaking voltage.

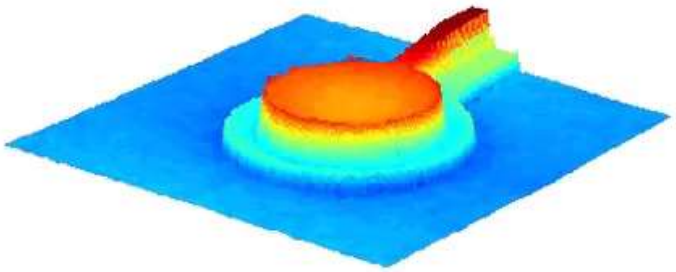

- DHM R1000
- Objectif:10x
- Operating mode: stroboscopic
- Driving signal: triangular
- Frequency 10Hz
- Voltage amplitude: 20,30,40V

Roughness

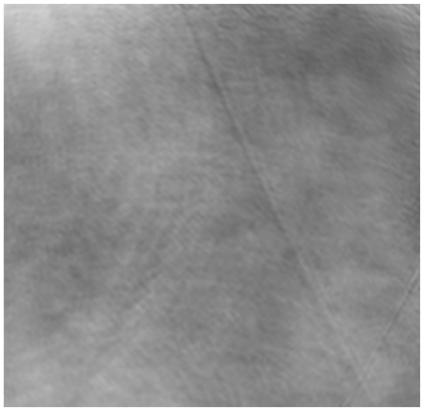

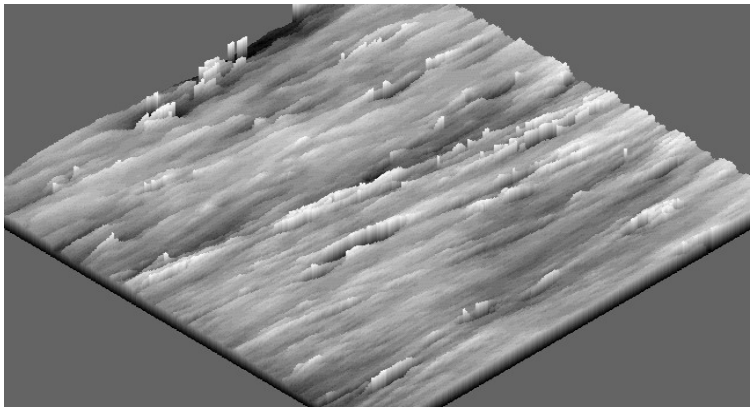

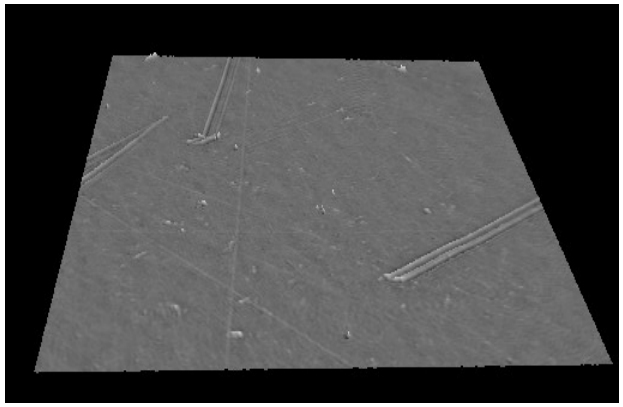

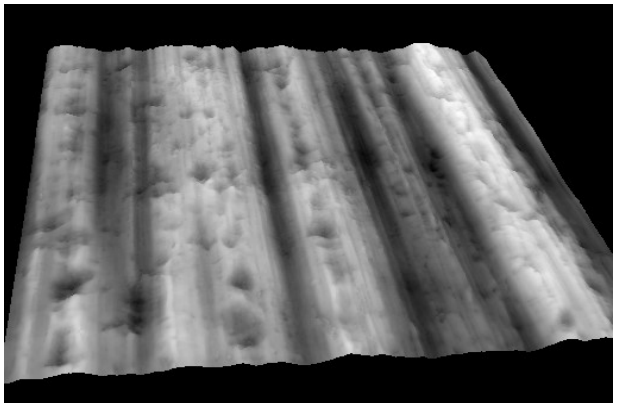

Roughness on curved surfaces

Metallic sphere (1 mm diameter)

- Phase image (modulo 2π)

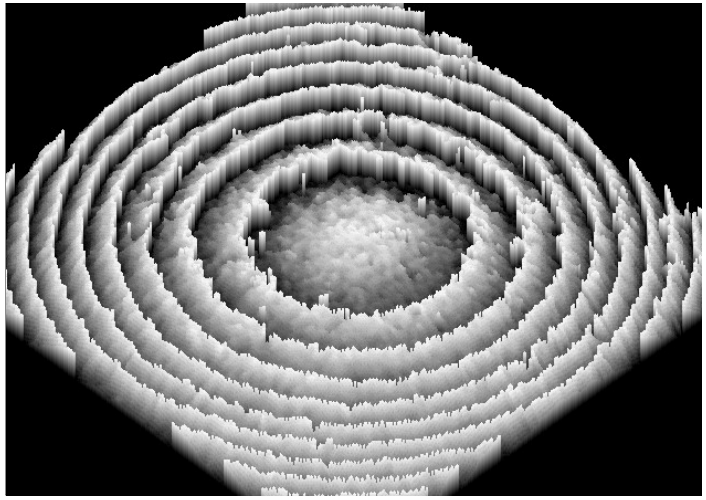

- Flattened surface

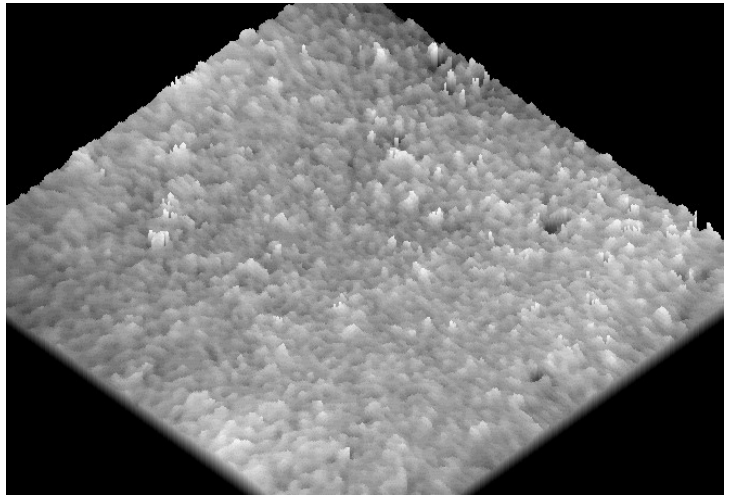

Micro-optics measurements

↳ Wrapped Phase

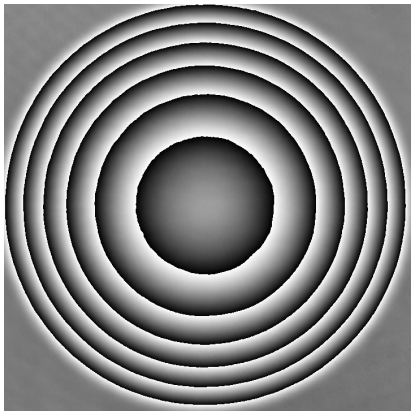

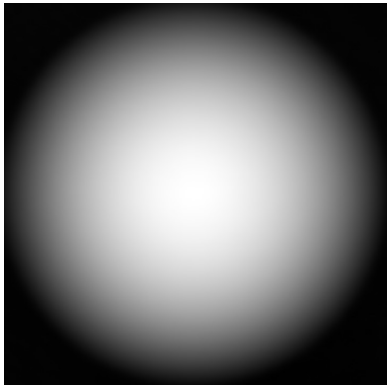

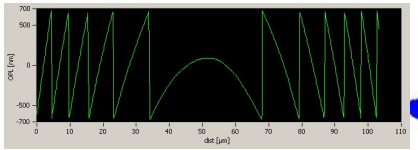

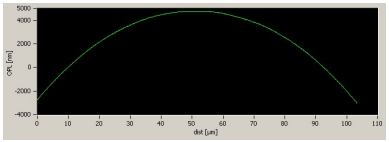

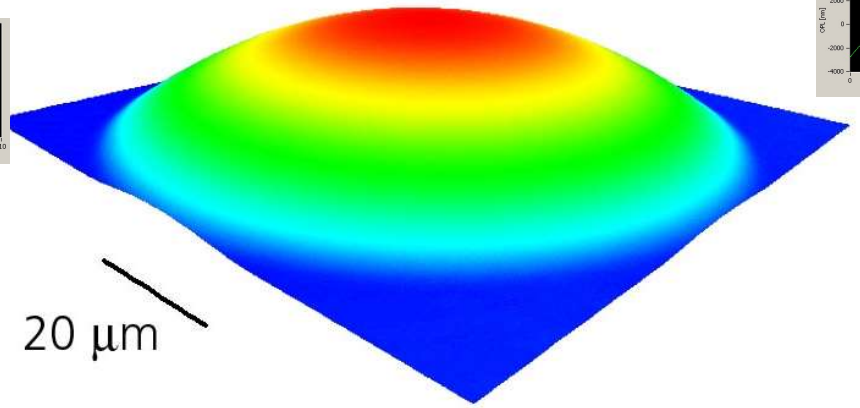

Micro-Optics

Diffractive elements

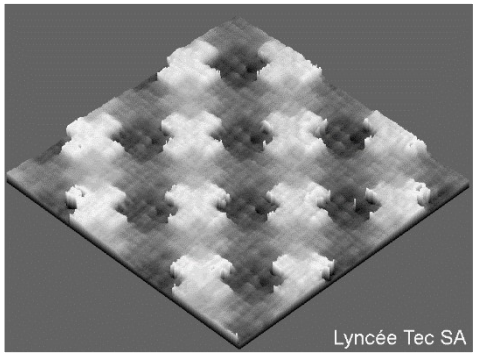

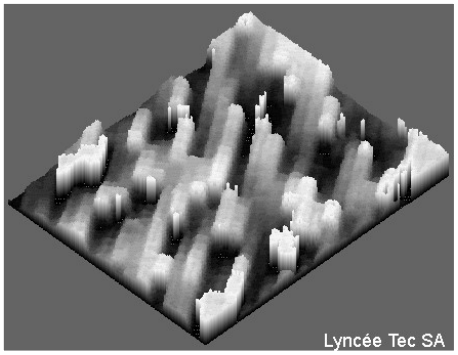

Fresnel Lens

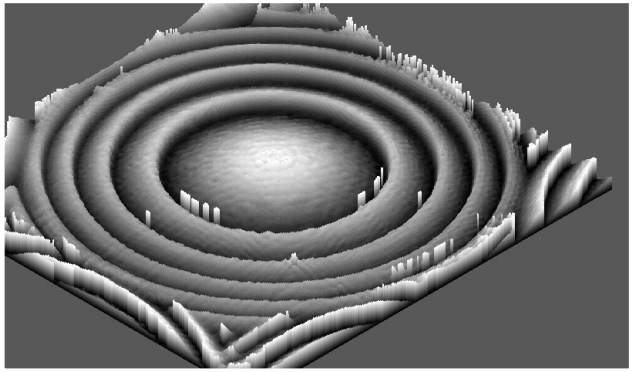

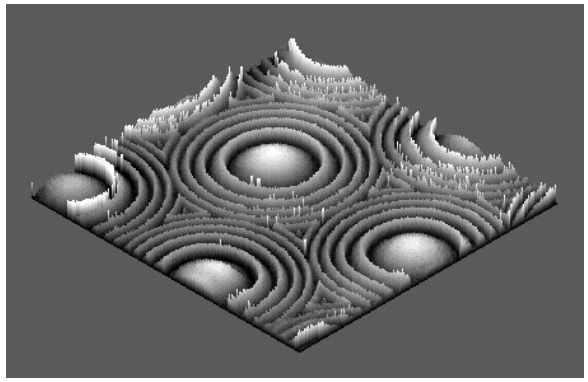

Sapphire: veils

- Crystalline defects

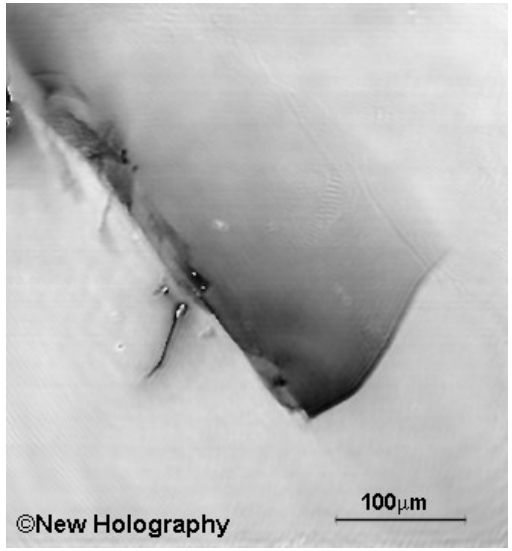

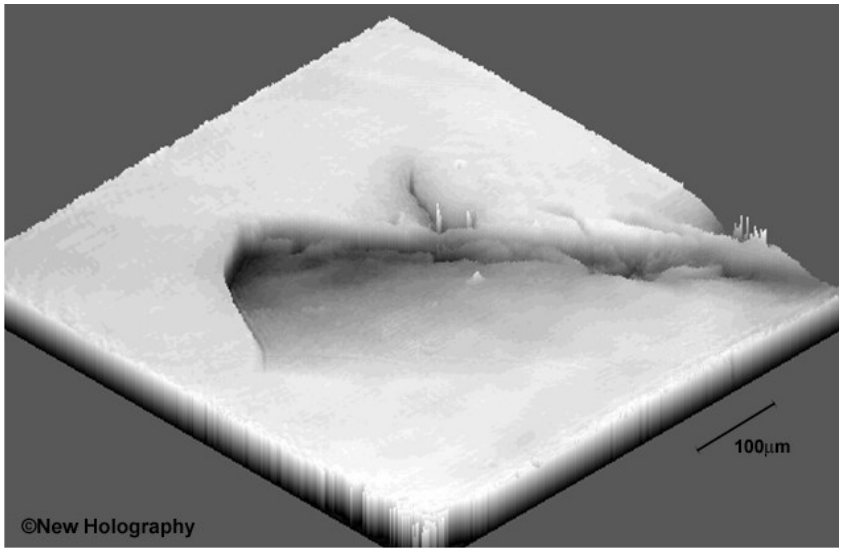

Cell morphology and dynamics

Light / Cell interaction

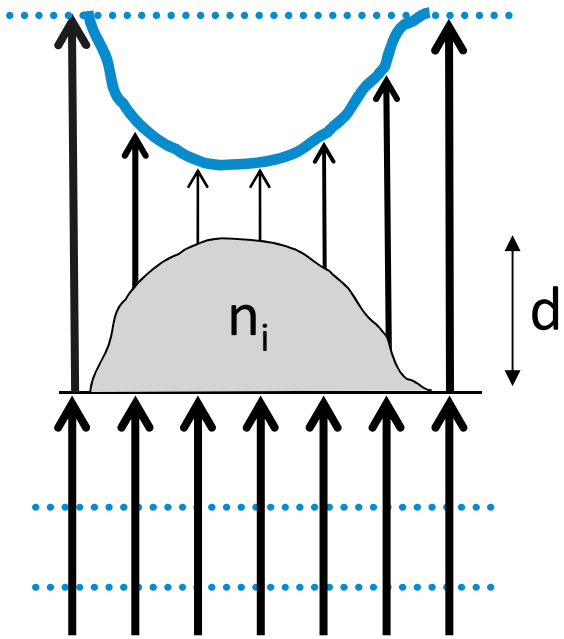

Living cells = weak scattering objects

Refractive index: $n=c/v$

c = speed of light in vacuum

v = speed of light in the considered medium

Wavefront φ modification:

$$\varphi \approx (d, n_i)$$

Quantitative Phase contrast image

Living cells in a perfusion chamber

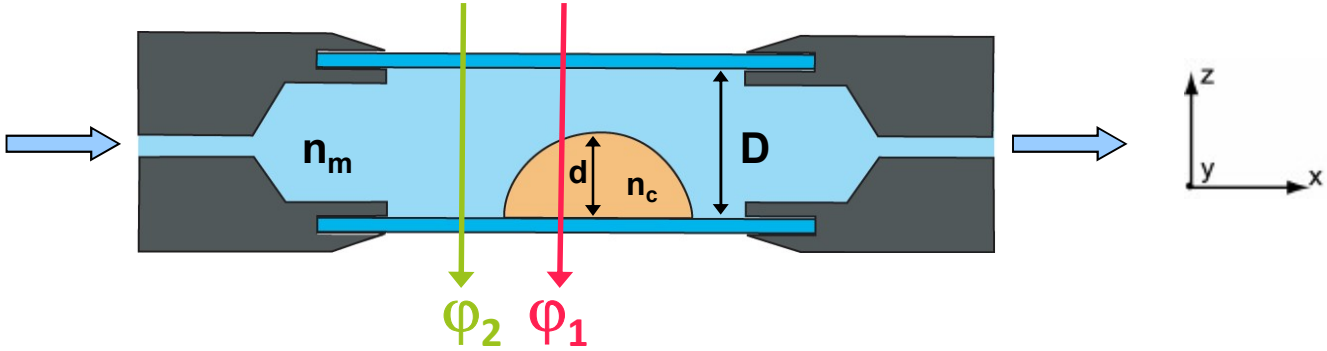

$$\Delta\varphi(x,y) = \varphi_1(x,y) - \varphi_2(x,y) = \frac{2\pi}{\lambda}(n_c - n_m)d(x,y)$$

Phase shift depends on both the **cell thickness** and the intracellular integral **refractive index**

$$n_c(x,y) := \frac{1}{d(x,y)} \int_{d(x,y)} n_c(x,y,z)dz$$

Phase sensitivity: σ = **0.1** Degree (λ/3600)

Perspective representation of a neuron

Measurement: $n_m = 1.3352 \pm 0.0002$
Assumption: $n_c = 1.365 \pm 0.01$

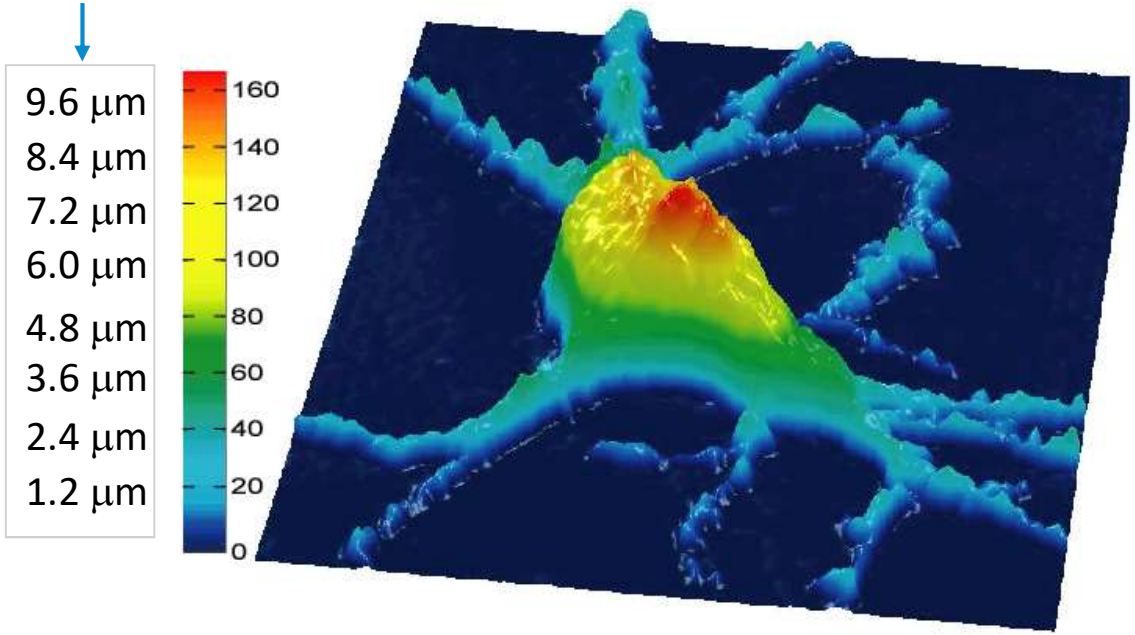

P. Marquet, Opt. Lett. 30 (5), 468-470 (2005)

Decoupling procedures

$$\varphi = \frac{2\pi}{\lambda}(n_c - n_m)d$$

Decoupling procedure

n_c: refractive index of the sample

d: thickness of the sample

Rappaz et al. Opt. Exp. 2005
Rappaz et al. Opt. Lett. 2008

Decoupling procedure

- Basic idea for decoupling phase signal:

  Recording two phase measurements for which RI of extracellular medium nm differs

  => Possibility to decouple phase signal

$$\varphi_1 = \frac{2\pi}{\lambda}(\boldsymbol{n_c} - n_{m1})\boldsymbol{d}$$

$$\varphi_2 = \frac{2\pi}{\lambda}(\boldsymbol{n_c} - n_{m2})\boldsymbol{d}$$

$$\longrightarrow$$

$$\boldsymbol{n_c} = \frac{\lambda_1\varphi_1 n_{m2} - \lambda_2\varphi_2 n_{m1}}{\lambda_1\varphi_1 - \lambda_2\varphi_2}$$

$$\boldsymbol{d} = \frac{\lambda_1\varphi_1 - \lambda_2\varphi_2}{2\pi(n_{m2} - n_{m1})}$$

Dye-enhanced dispersion of perfusion medium

Decoupling strategies

- Implementation of decoupling: Acquire holograms at two different wavelengths λ_1, λ_2 for which extracellular solution medium shows a high RI dispersion

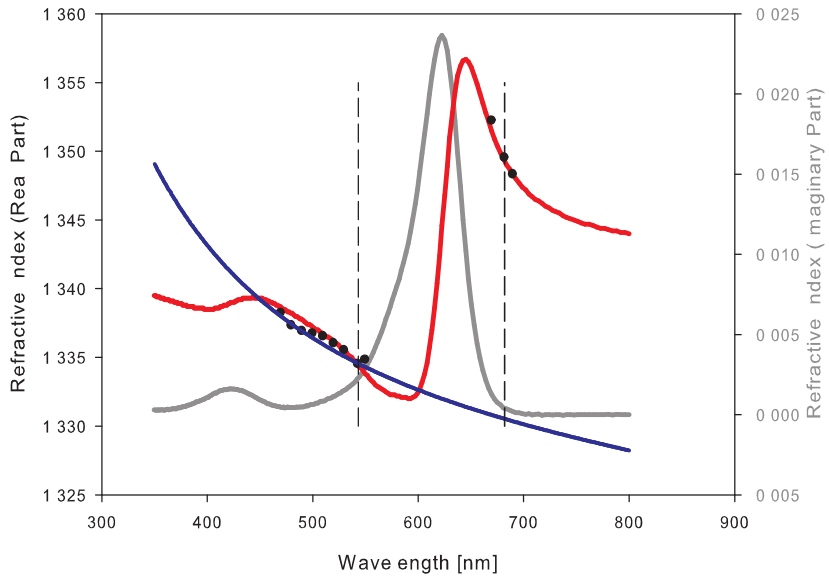

Imaginary Part RI Fast Green 20 mM
Real Part RI Fast Green 20 mM
RI Water

Requirements of Dye:

High solubility in water
Nontoxic for living cells
No diffusion across cellular membrane
-> Fast Green Dye

Rappaz, B. et al., Opt. Lett. 33(7), 744–746 (2008)

Simultaneous decoupling strategies

Dual-wavelength hologram

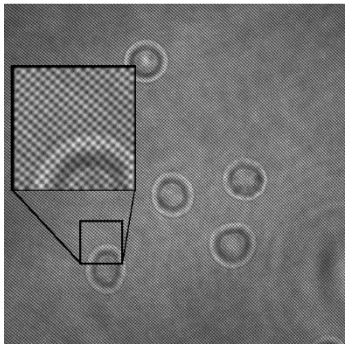

Hologram Fourier-Space

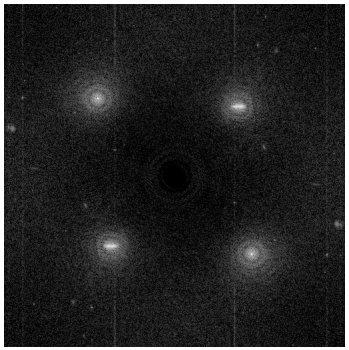

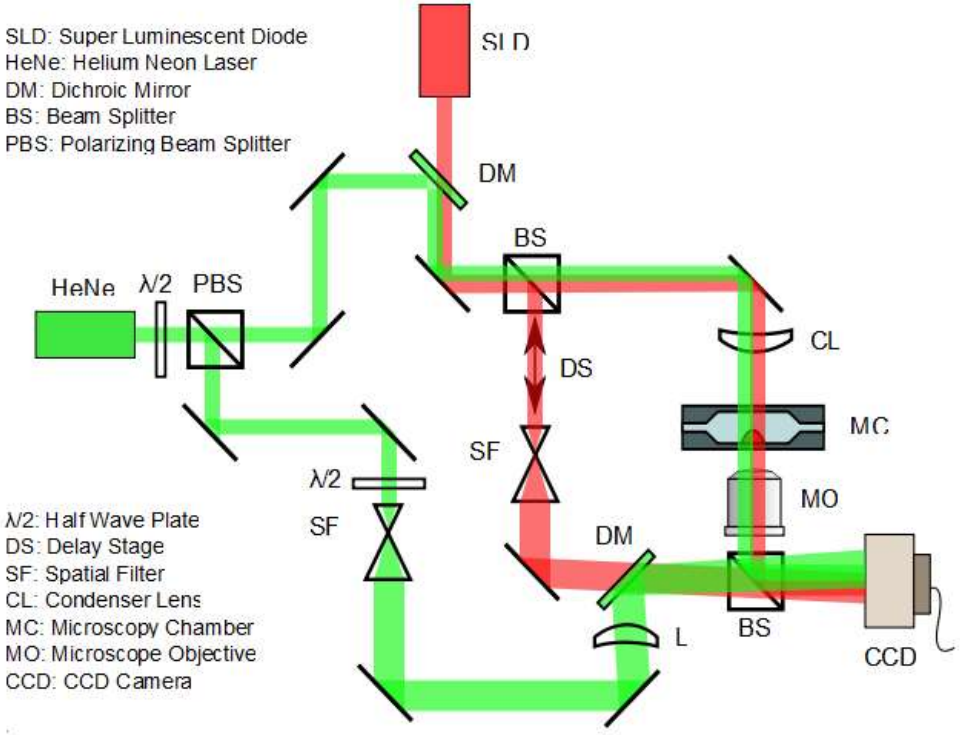

Kühn, J. et al., Opt. Express 15(12),7231–7242 (2007)

Hematological parameters measured in RBC

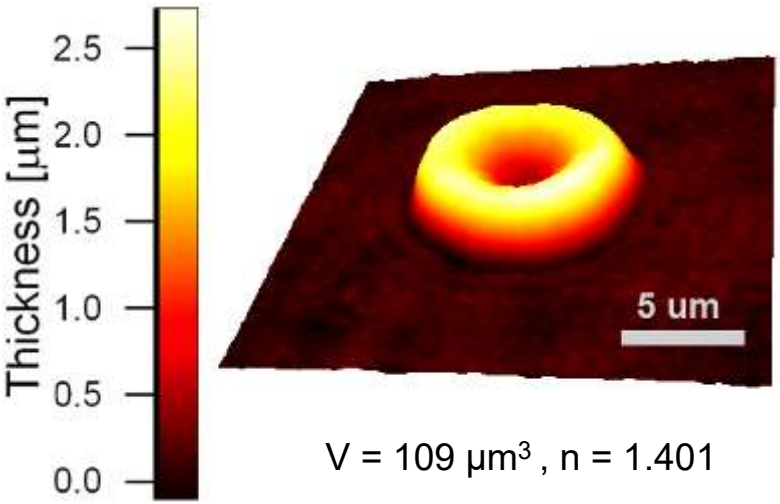

V = 109 µm^3 , n = 1.401

	Mean	SD
Mean corpuscular volume (MCV) [fL]	**86**	15.2
Refractive index (RI)	**1.418**	0.008
Diameter [mm]	7.8	0.5

Result of the decoupling procedure expressed as mean and standard deviation (n = 34 erythrocytes measured)

Mean corpuscular Hb (MCH) : 29.9 pg

MCHC:=MCH/MCV= 362 ± 8 g/l

MCV and MCHC are important clinical parameters to monitor in various blood diseases.

Rappaz et al., Cytometry (2009)

Fluctuation of cell membrane

- RBC membrane
  - Lipid bilayer + spectrin skeleton
  - Deformation to squeeze through small capillaries
  - Flicker phenomenon
  - Debate on the origin of this cell membrane fluctuations CMF

Advantages of DHM: non-disturbing measurement in the nanometer and microsecond range, whole cell surface

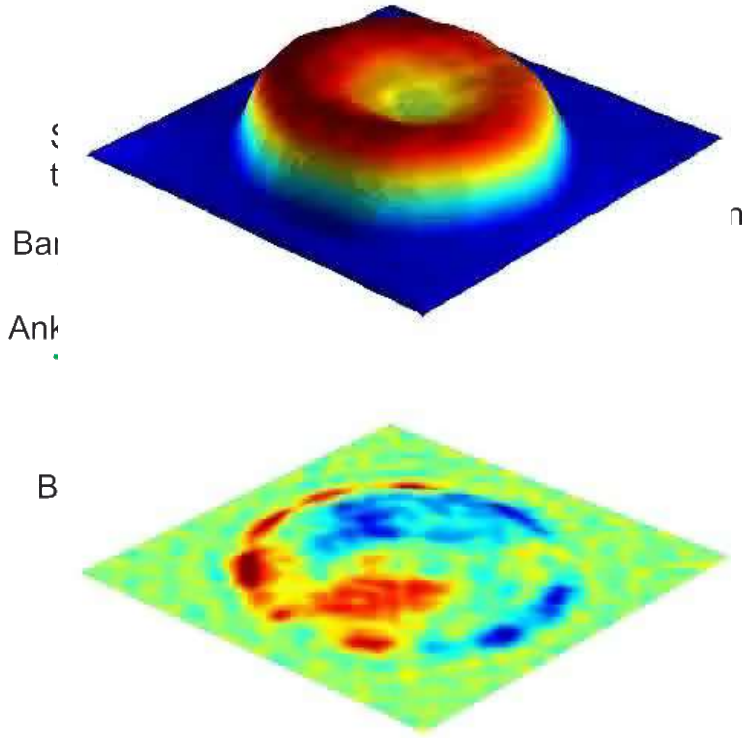

B. Rappaz, Blood Cells Mol Dis. Mar 24 (2009)

Principal component analysis (PCA)

- **PCA:** simplifying the data into the significant components responsible for the movement of the membrane and removing the negligible parts and experimental noise

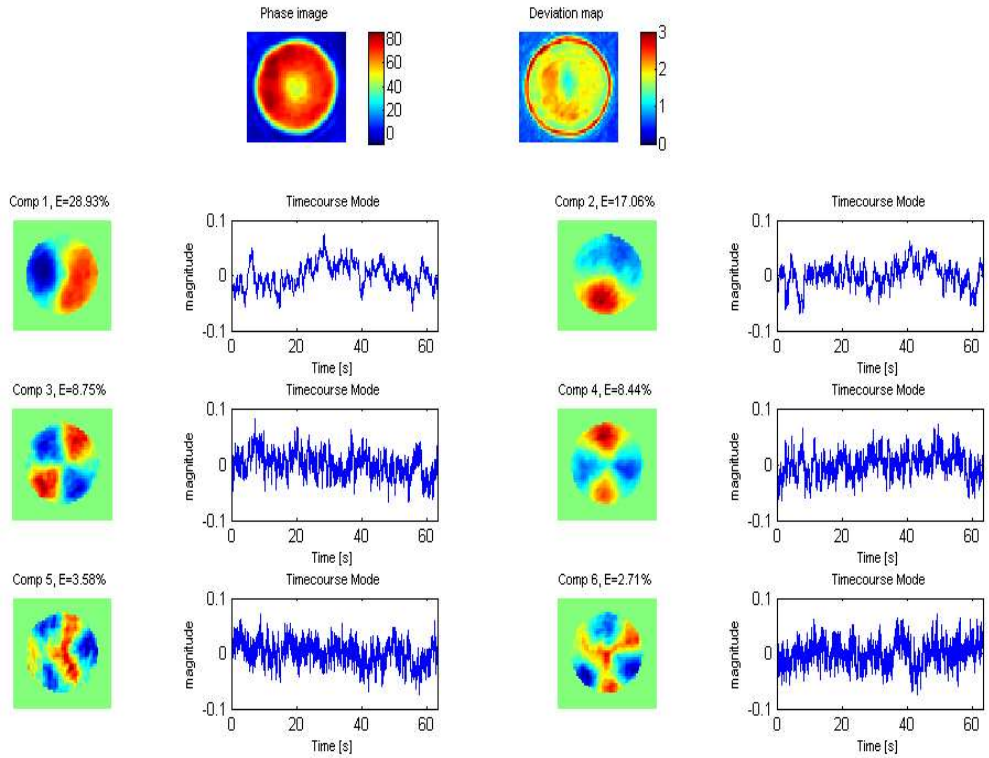

Origin of the RBC flickering

Group analysis PCA (n=198)

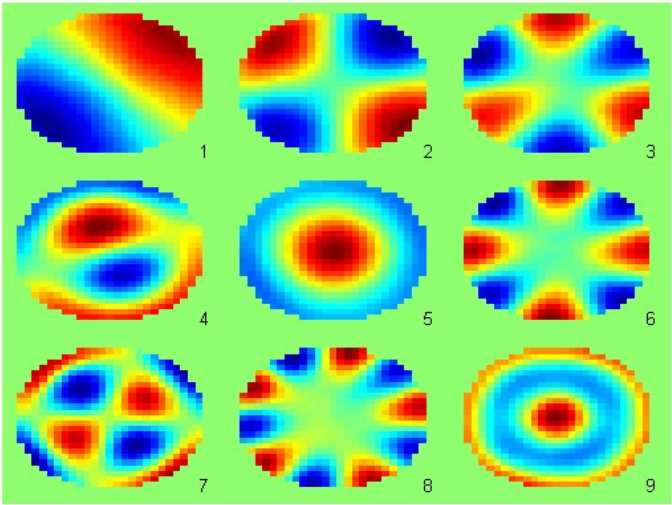

PCA modes

Bending modulus: **= (2.75±0.78) 10−19J**

Thermal origin of the RBC flickering!

Minimal model :

- Typical biconcave form
- Bending elasticity of the membrane

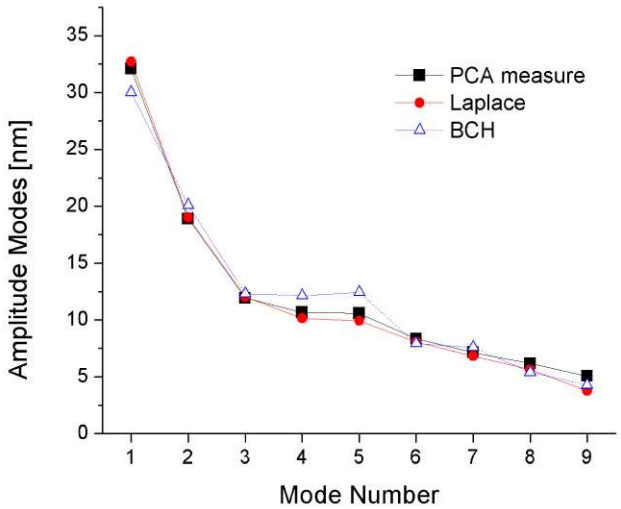

Eigenmodes

Energy distribution of the PCA modes are in good agreement with the equipartition theorem

D. Boss, PLos One (2012)

Identification of cell biomarkers

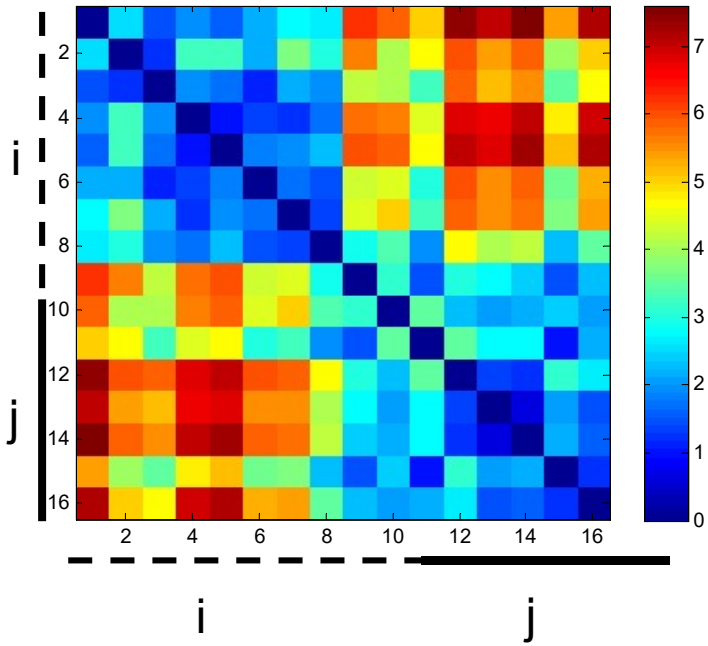

j = 1..8 Healthy subjects

i = 8..16 Diabetic patients

Each t-value (i,j) in the matrix indicates how similar the energy distribution of the PCA modes between subject *i* and subject *j* are. The lower this t-value, the more similar the energy distribution is.

-> Healthy and diabetic populations can be distinguished. Correlation between mode Energy distribution and HbAc1 fraction is currently analyzing.

t-value > threshold

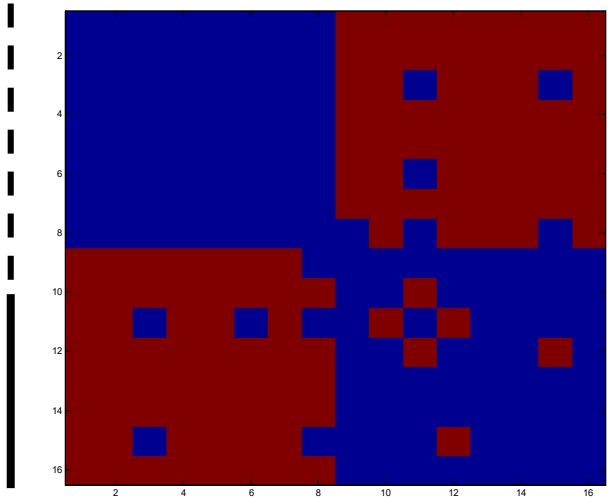

High sensitivity of QPS to water movements

- Variation of the phrase (φ) during an hypotonic shock on neurones

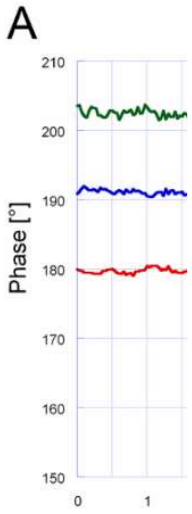

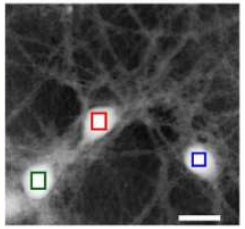

$$\varphi = \frac{2\pi}{\lambda}(n_c \downarrow - n_m)d \uparrow$$

Water Influx

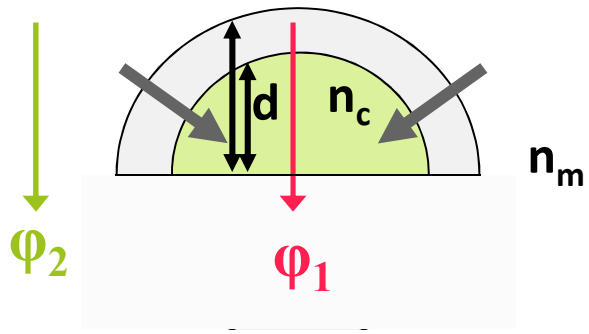

Measurement of water transmembrane permeability

- The osmotic water membrane permeability P_f of a semi-permeable membrane determines the **water volume flux** [per unit of time per unit of membrane surface] for a given applied osmotic gradient

$$P_f = \frac{1}{v_w A_0 \Delta\Pi_0}\left(\frac{\partial V}{\partial t}\right)_0 = \frac{\Delta V}{\tau v_w A_0 \Delta\Pi_0}$$

  - osmotic gradient between intra- and extracellular compartments $\Delta\Pi_0$
  - partial molar volume of water v_w
  - cell surface area A_0
  - change rate of the initial cell volume $\left(\frac{\partial V}{\partial t}\right)_0$

Cell surface can be calculated from the cell thickness measurement

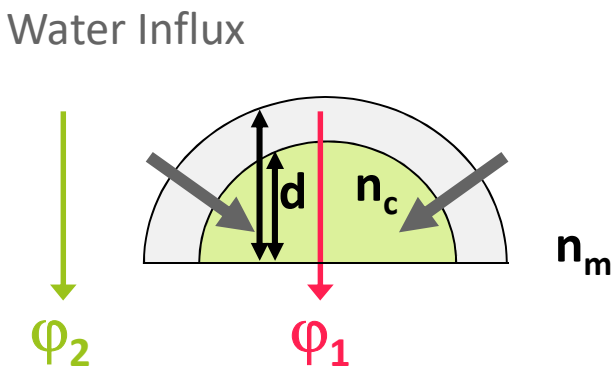

Initially 300 mOsm
At t_0: 150 mOsm

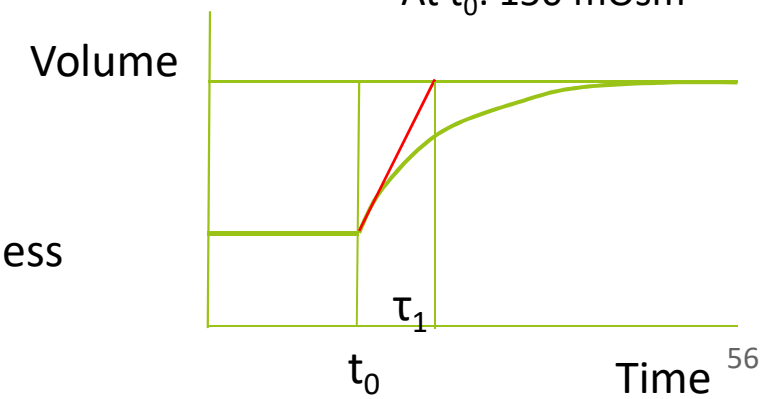

D Boss et al., JBO (2013)

	V_0 $[\mu m^3]$	ΔV $[\mu m^3]$	$(\Delta V + V_0)/V_0$	Π_i/Π_o	$A_0[\mu m^2]$	τ [s]	P_f $[10e-3cm/s]$
CHO	1660±669	718±294	1.4341±0.065	1.452	747±340	33.71±5.6	1.65±0.318
HEK	1996±562	1437±377	1.739±0.16	1.667	676±153	34.6±10.9	3.04±0.87
Neuron	1671±1116	609±429	1.376±0.09	1.452	475±226	17.8±8.42	4.69±2.89
Astrocyte	861±324	347±132	1.463±0.319	1.452	475±137	6.44±2.78	7.64±3.54

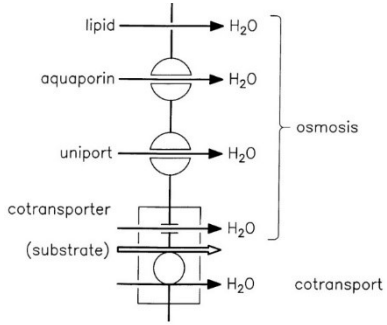

Osmotic water membrane permeability for various cellular types

QP-DHM to explore cell dynamics

- Membranes of animal cells are highly permeable to water
- Movements of water across membranes are therefore dictated in large part by osmotic pressure gradients
- At constant extracellular osmolarity, volume constancy of any mammalian cell is permanently challenged by its physiological and pathophysiological activity

Measurements of both **cell volume** and **transmembrane water movements** allow to characterize cell activity, identify new cell biomarkers of diseases as well as reveal new insights into pathophysiology

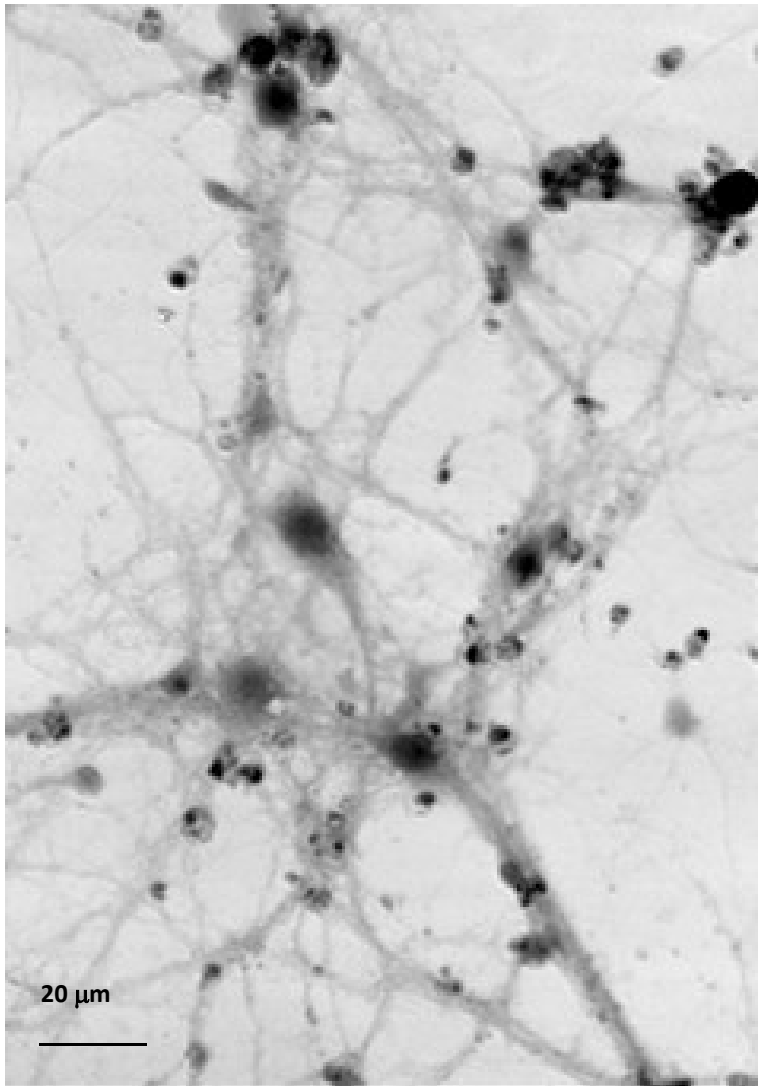

Resolving neuronal network activity

Quantitative phase image of primary culture of mouse cortical neuronal

Neuronal activity (firing) mediated by glutamate

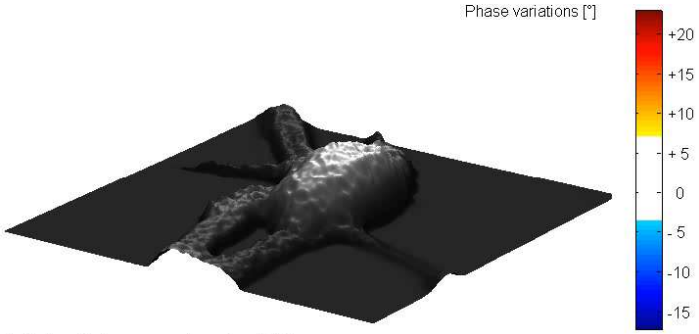

Initial cell phase contrast = 197°

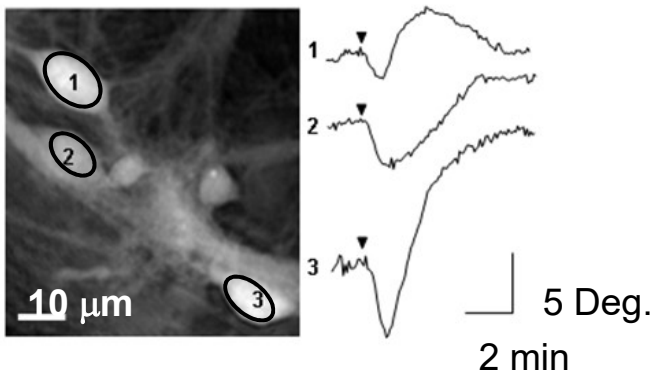

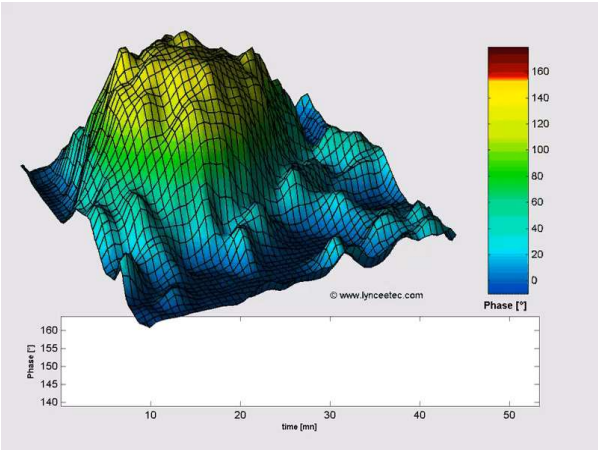

Three types of responses:

- biphasic
- reversible
- irreversible

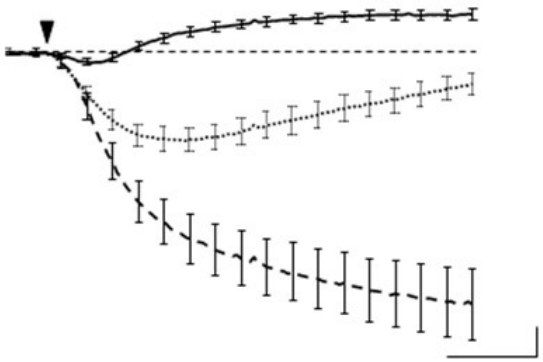

Neuronal excito-toxicity mediated by glutamate

Glutamate excito-toxicity

3

Three types of responses:

- biphasic
- reversible
- irreversible

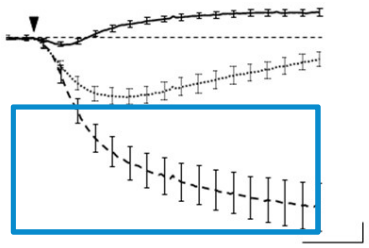

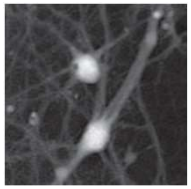

		S_{cell} [µm²]	V_{cell} [µm³]	Mean Intracellular RI
Initial	cell 1	129 ± 20	1332 ± 230	1.365 ± 0.0003
	cell 2	162 ± 22	1412 ± 217	1.364 ± 0.0003
Excitotoxic	cell 1	210 ± 25	2106 ± 285	1.351 ± 0.0003
	cell 2	260 ± 28	2196 ± 280	1.353 ± 0.0003

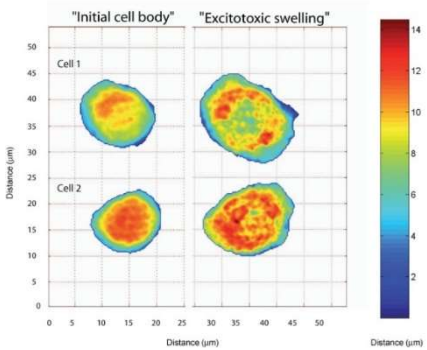

Pavillon et al., J. of Biophotonics (2010)

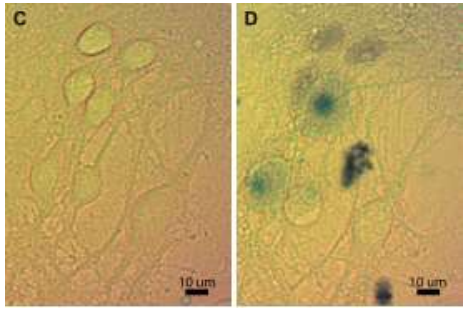

Pavillon et al. PLoS One (2012)

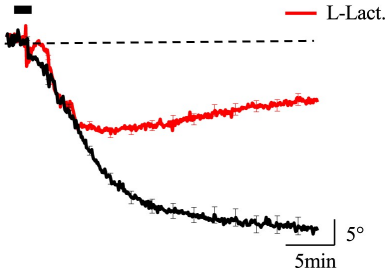

Jourdain et al. Sci. Reports (2016)

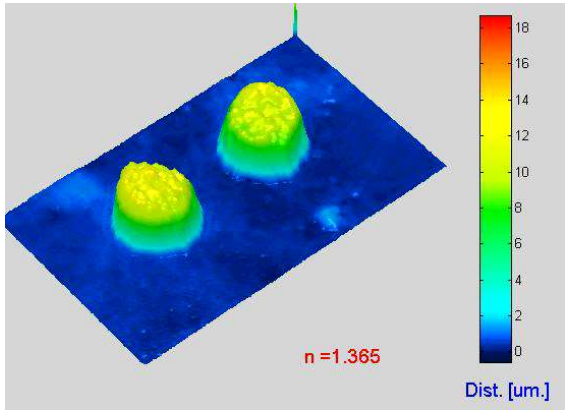

Deconstructing neuronal activity (firing) mediated by glutamate

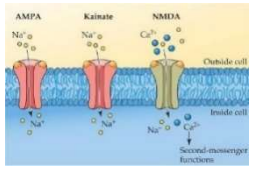

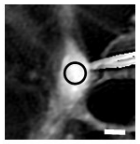

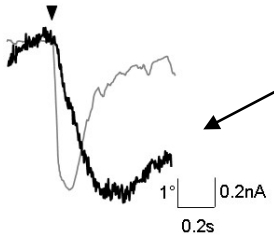

rapid transient phase decrease associated with an inward current

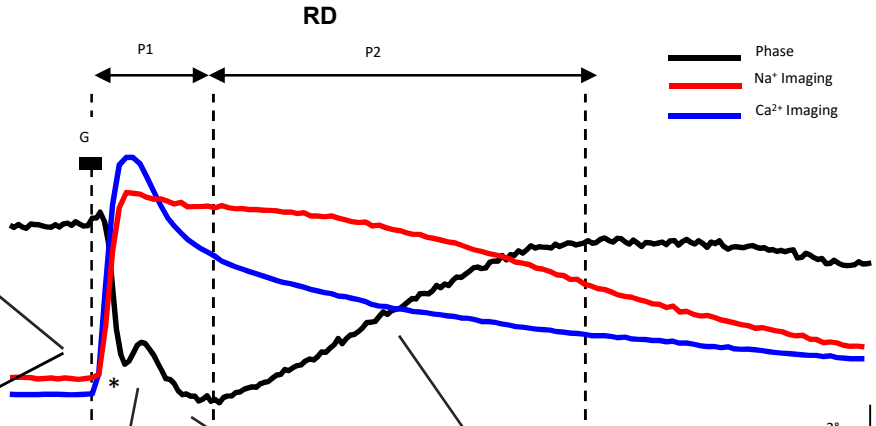

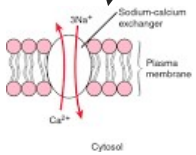

Exchanger $3Na^+/Ca^{2+}$

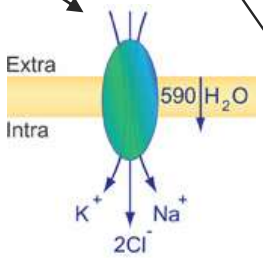

NKCC1

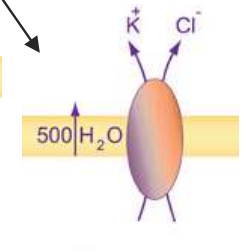

KCC2

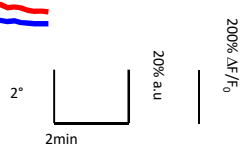


The Journal of Neuroscience
www.jneurosci.org

The Journal of Neuroscience, **17 August 2011**, 31(33): **11846-11854**; doi: 10.1523/JNEUROSCI.0286-11.2011

Cellular/Molecular

Determination of Transmembrane Water Fluxes in Neurons Elicited by Glutamate Ionotropic Receptors and by the Cotransporters KCC2 and NKCC1: A Digital Holographic Microscopy Study

Pascal Jourdain[1], Nicolas Pavillon[2], Corinne Moratal[1], Daniel Boss[1], Benjamin Rappaz[1], Christian Depeursinge[2], Pierre Marquet[1,3,*], and Pierre J. Magistretti[1,3,*]

Experiments combining DHM and electrophysiology set-up

Electrophysiology

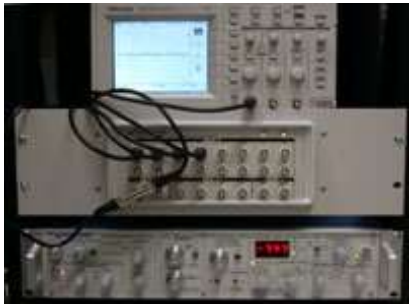

DHM/Electrophysiology set-up

DHM

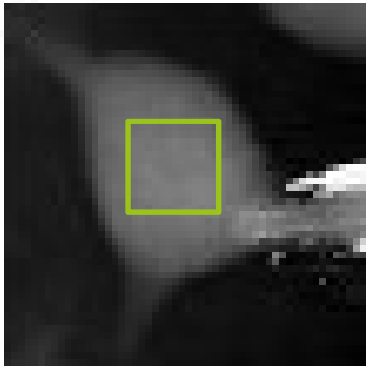

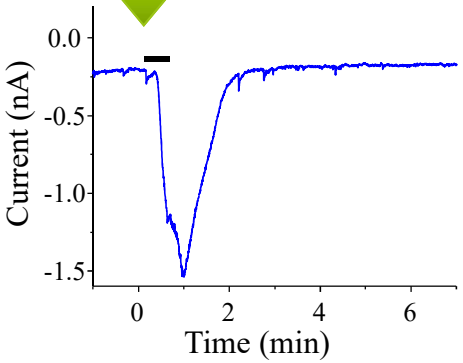

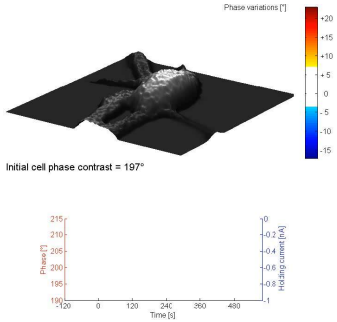

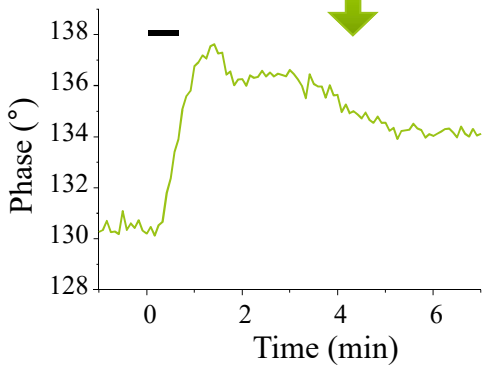

Membrane current derived from measured phase signal

- Assumptions:

$$n_{cell} \propto \alpha C \qquad \Delta V_{cell} \propto Q = \int I dt$$

$$\varphi = \frac{2\pi}{\lambda}(\boldsymbol{n_c} - n_m)\boldsymbol{d}$$

n_{cell} = intracellular refractive index
C = intracellular constituent concentrations [g/l]
α = specific refraction increment [l/g] (Barer et al 1952)
ΔV_{cell} = cell volume variation
Q = net charges having passed through the membranes [nC]
I = current [nA]

Membrane current derived from measured phase signal

$$I_{Glut}(t) = \frac{V_0}{\varepsilon}\frac{d}{dt}\left(\frac{\varphi_0}{\varphi(t)}\right)^{1/1-r}$$

P. Jourdain et al. , PLos One, 2012

$\phi(t)$= phase signal [Deg.]
I = current [nA]
ϕ_0= initial phase signal
V_0 = initial cell volume [l]
ε= volume variation per number of net transported charges [l/nC]
r= 1/3 isotropy volume variation (r=0.7 neuron)

Identifying new cell biomarkers

Fluorescence

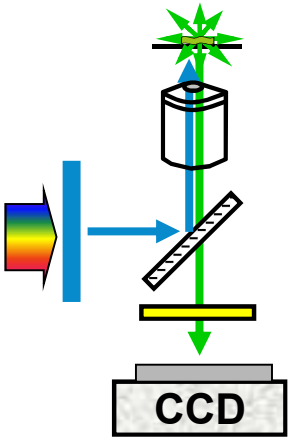

Set of various cell parameters characterizing a **cell dynamic phenotype**

Morphology, volume, changes, water permeability, transmembrane water movements

Membrane fluctuations and biomechanical properties, etc.

Diffraction Tomography

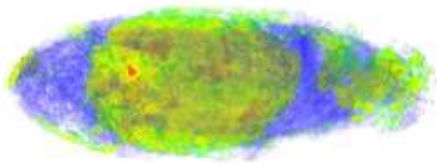

DHM

Human cellular Reprogramming

To create patient-derived cells

- Induced pluripotent stem cells (Yamaka, Nobel prize, 2006)

Nonlinear optics

(SHG, THG, CARS etc..)

Screening capabilities

Automation and parallelization

- Fast reading of well plates
- …

Tomography

Phase microscopy

- Signal: coherently scattered field
  - Amplitude and Phase
  - Wavefront

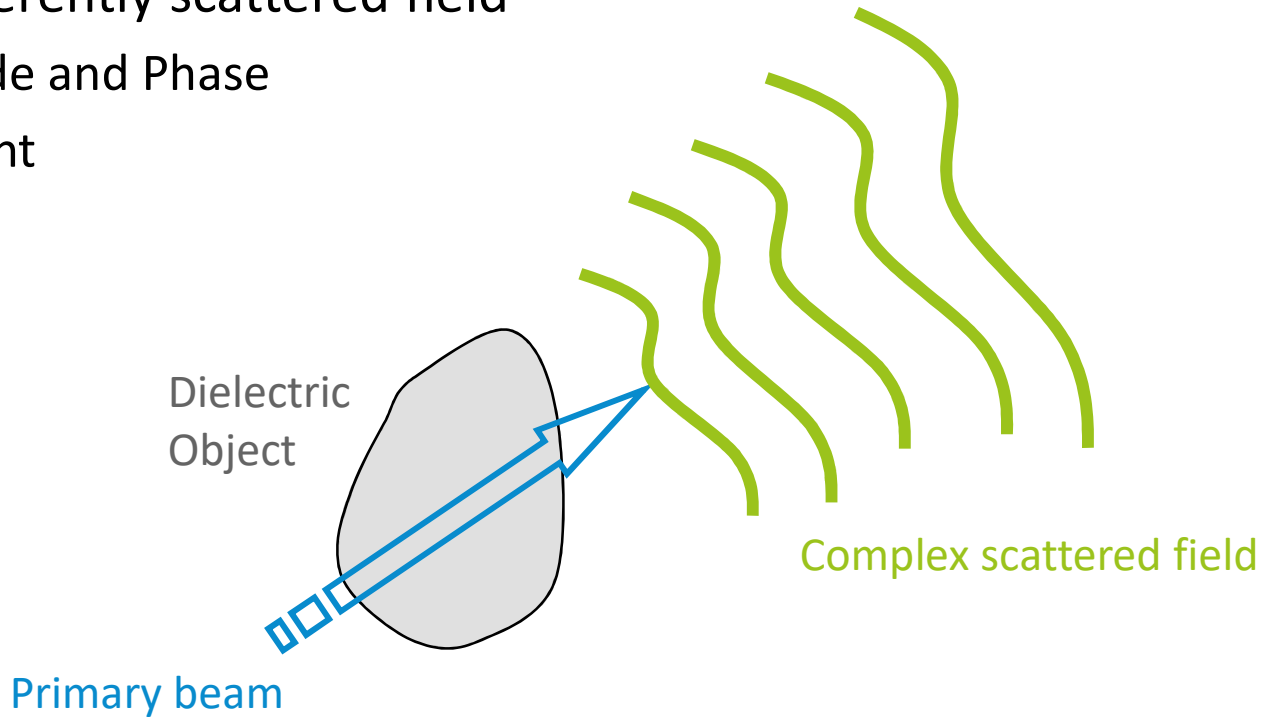

A fundamental theorem: diffraction tomography

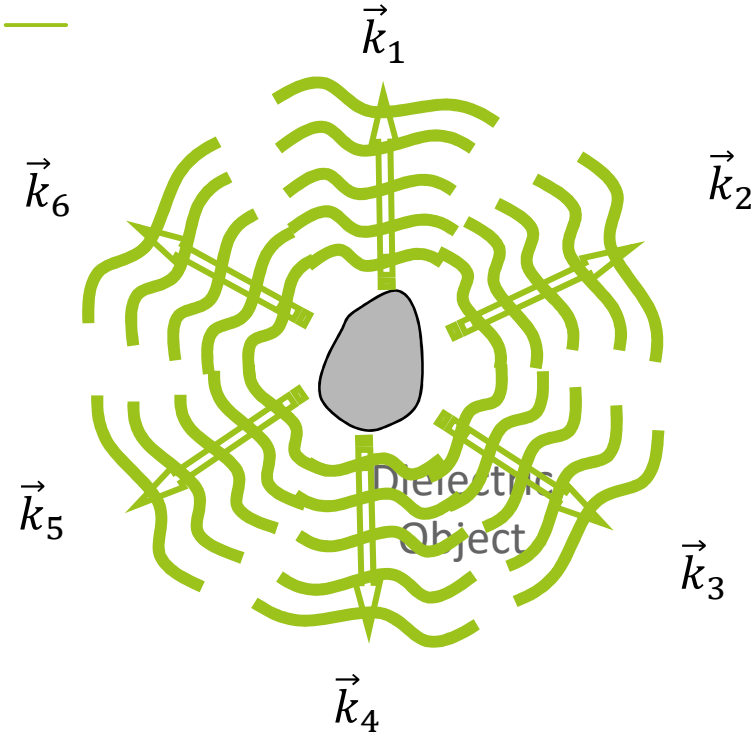

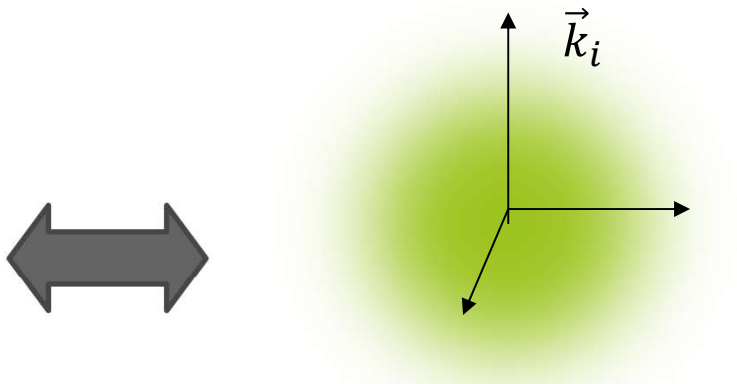

Photonic field in the Fourier space

A full combination of generated illumination fields and measured scattered fields allow for populating fully the Fourier image of the scattered potential, from which the RI is computed

$\Delta\vec{x} \downarrow\downarrow$ $\quad \Delta\vec{k}\Delta\vec{x} = cte \quad$ $\Delta\vec{k} \uparrow\uparrow$

- Photonic field in the real 3D space:
  - Field measurement for a plurality of illuminating fields

Enlargement of the spatial spectral domain by rotation of the illuminating beam

- Rotating the illuminating beam allows synthesizing a larger aperture of the microscope objective

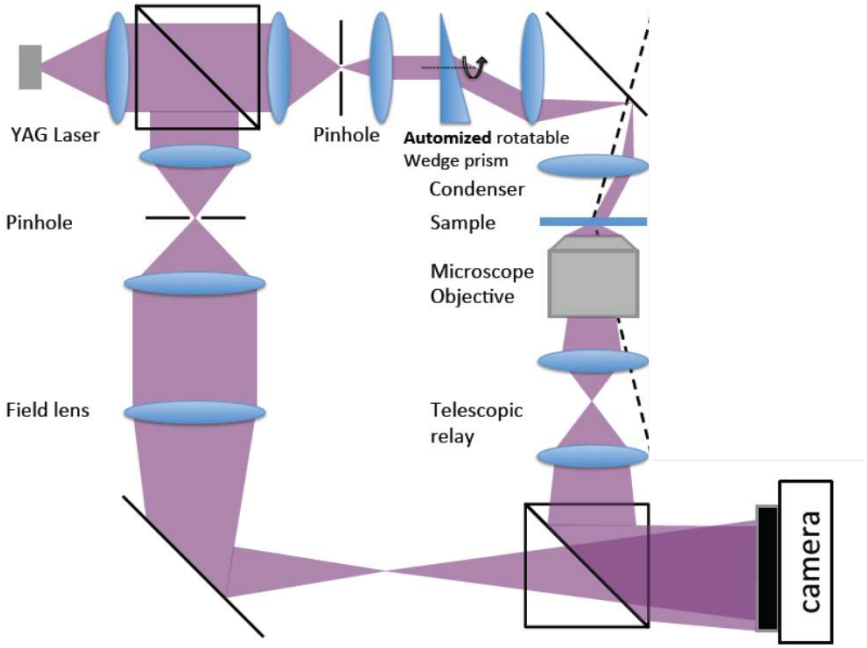

Cotte et al. Nature photonics (2013)

Multi-incidence full 3D tomography

- Rotating the sample allows for achieving full diffraction tomography

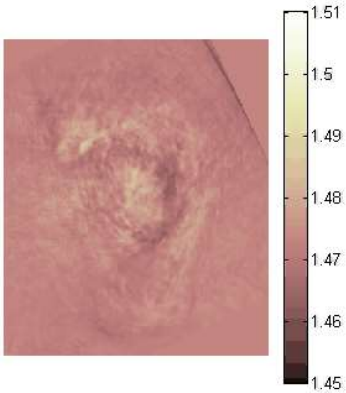

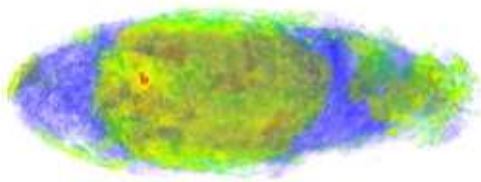

Florian Charrière et Al.
(Optics Express 7011- Vol. 14, No. 16 - 7 August 2006)

Lauer 2002
Price 2006
Choï 2007
Vertu 2008
Sung 2009
Debailleul 2009
Cotte 2011
…

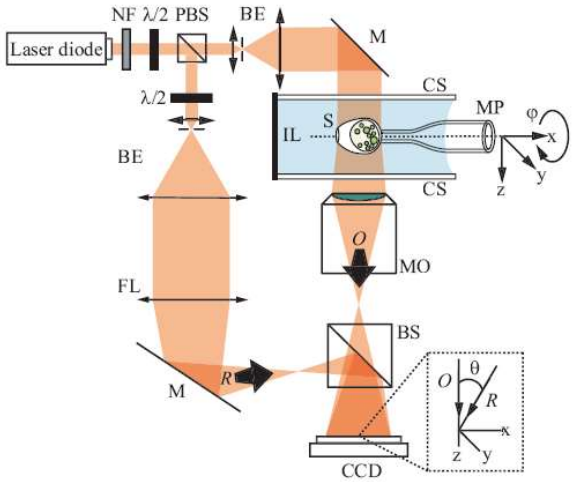

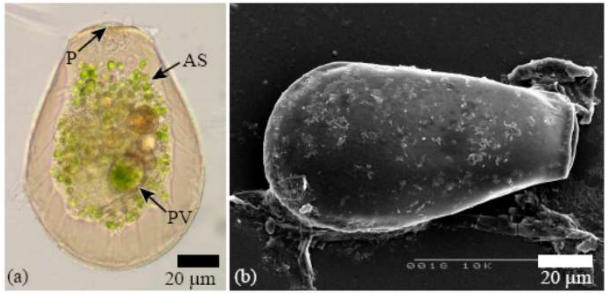

Images of the testate amoebae Hyalospheni apapilio:
(a) bright-field microscope image illustrating the amoeba itself and its content
P pseudostome (opening through which the amoeba pseudopods emerge),
AS algal symbionts,
PV phagocytic vacuoles;
(b) SEM image illustrating the shell.

Primary culture of mouse cortical neurons

- Spatial averaging of noise reduces phase noise by one order of magnitude

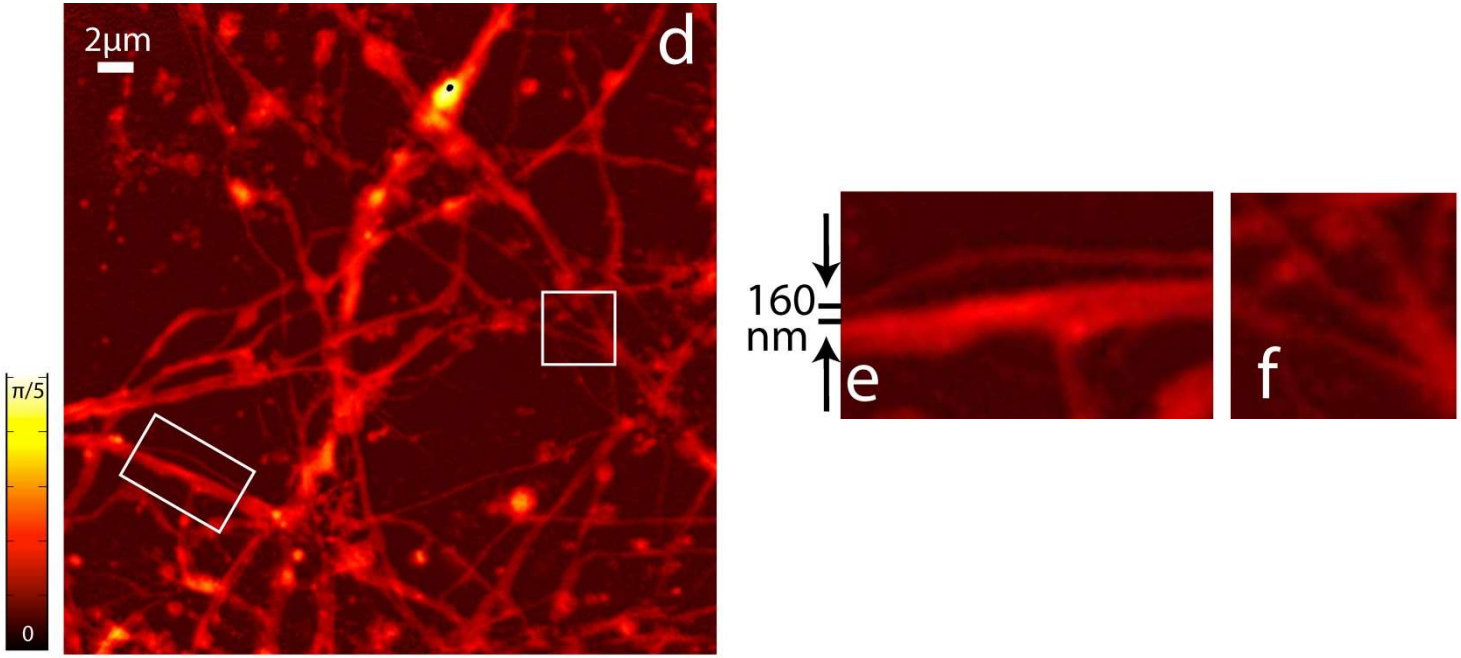

Glutamate mediated dendritic spine dynamics

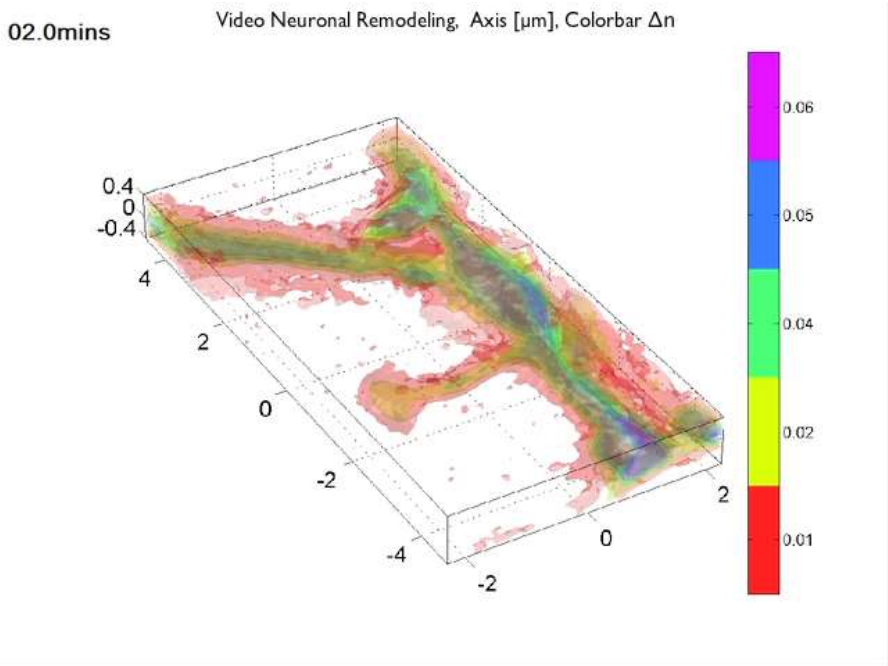

Cotte et al. Nature photonics (2013)

The Lausanne team

Neurophotonics group, UNIL
Kaspar Rothenfusser
Kévin Bourgeaux
Stéphane Chamot
Pierre Marquet

Brain and Mind Institute, EPFL
Pascal Jourdain
Christian Depeursinge
Pierre J. Magistretti




Biomolecular Screening Facility, EPFL
Gerardo Turcatti
Benjamin Rappaz


Lyncée Tec SA
Etienne Cuche
Tristan Colomb
Yves Emery



The Québec team

Psychiatry and Neurophotonics Research Laboratory (Dr. Pierre Marquet)

Erik Bélanger, PhD
Valérie Chénard, MSc
Ana Sofia Correia, PhD
Issam Derouiche
Antoine Godin, PhD
Sébastien Lévesque, PhD
Jean-Michel Mugnes, PhD
Anne-Sophie Poulin-Girard, PhD
Martin Roy, PhD
Nathalie Van Houtte
Pierre-Louis Gagnon
Fariborz Khademian
Celedonia Krawczyk
Sara Mattar
Niraj Patel
Charles Pichette
Philippe Bilodeau
Bertrand de Dorlodot
Andréanne Deschenes
Antoine Grégoire
Pauline Lavergne
Yasmine Alikacem
Vincent Clément
Louis D'Amour
Alexis Lebrun
Émile Rioux-Pellerin
Valérie Watters

CIUSSS-CN Centre de neuromédecine personnalisée et du développement de l'enfant (Dr. Michel Maziade)

Elsa Gilbert, PhD
Thomas Paccalet, PhD
Byanka Lagacé, BSc inf
Geneviève Poirier, BSc inf
Joanne Lavoie, MSc inf
Valérie Beaupré Monfette
Emilie Binet
Marie-Claude Boisvert
Daphné Lussier
Linda René

Centre intégré universitaire de santé et de services sociaux de la Capitale-Nationale Québec

LRNP
COPL Centre d'optique, photonique et laser
CENTRE DE RECHERCHE CERVO BRAIN RESEARCH CENTRE QUÉBEC
UNIVERSITÉ LAVAL
Canada Excellence Research Chairs
Chaires d'excellence en recherche du Canada